DEGREE PROJECT IN ELECTRICAL ENGINEERING,
SECOND CYCLE, 30 CREDITS
STOCKHOLM, SWEDEN 2020

Dual-polarized feed for mmWave lens antennas

JUAN LUIS ALBADALEJO-LIJARCIO

KTH ROYAL INSTITUTE OF TECHNOLOGY
SCHOOL OF ELECTRICAL ENGINEERING AND COMPUTER SCIENCE

Dual-polarized feed for mmWave lens antennas

Juan Luis Albadalejo Lijarcio

Examiner

Oscar Quevedo Teruel (KTH Royal Institute of Technology)

Supervisors

Oskar Zetterström (KTH Royal Institute of Technology)

Elena Pucci (Ericsson)

Darwin Blanco (Ericsson)

Lluis Jofre Roca (UPC Polytechnic University of Catalonia)

May 2020

Abstract

The fact of being bulky and not very cost-efficient made lens antennas not to be taken much into account in the past. Nowadays, this kind of antennas has attracted more attention due to the increasing demand of higher frequencies in 5G, where lenses become considerably smaller. Moreover, the advances achieved in manufacturing techniques such as 3D printing have reduced the costs to a great extent. Lenses can be used to transform the Electromagnetic (EM) waves coming from a source into any desired radiation pattern. For example, a directive beam in any specific direction could counteract the higher path losses at the new frequency bands used in 5G.

In order to feed the lens, a transition from a coaxial cable to a waveguide or horn antenna working at the desired frequency band has been used as the source. However, most of the time, these feeds are only able to support a single polarization, thus not exploiting the capabilities, such as the increase in capacity, of using Polarization-Division Multiplexing (PDM).

In this thesis, a system composed of a dual-polarized array feed and a Gutman lens operating at the frequency band of 28 GHz is designed and simulated in order to analyze its performance. Commercial software CST Microwave Studio is used for that purpose. Some prototype ideas to be manufactured in the future are also analyzed.

Abstract

El hecho de ser voluminosas y no muy rentables hizo que las antenas de lente no fueran tenidas muy en cuenta en el pasado. En la actualidad, este tipo de antenas ha ganado una gran atención debido a la creciente demanda de frequencias más altas en 5G, donde las lentes son considerablemente más pequeñas.. Además, los avances conseguidos en ténicas de fabricación como la impresión 3D han permitido reducir los costes de fabricación en gran medida. Las lentes pueden ser utilizadas para transformar las ondas electromagnéticas de una fuente en cualquier patrón de radiación deseado. Por ejemplo, un haz muy directivo en una dirección específica podría contrarrestar el incremento en las perdidas de propagación en las nuevas bandas de frecuencia usadas en 5G. También se analizan algunas de las ideas de prototipos a ser fabricados en el futuro.

Para alimentar la lente, normalmente se ha utilizado como fuente una transición de un cable coaxial a una guia de onda o antena de bocina operando en la banda de frecuencia deseada. Sin embargo, en la mayoría de las ocasiones, estas fuentes son solo capaces de funcionar con una única polarización y por lo tanto, no acaban explotando las posibilidades, como el incremento en la capacidad, al usar Multiplexación por División de Polarización (PDM).

Un sistema compuesto por un array de antenas dualmente polarizadas y una lente de Gutman funcionando en la banda de frecuencia de 28 GHz es diseñado en este trabajo final de máster. El software comercial CST Microwave Studio es utilizado para tal propósito. Algunas ideas de prototipos para ser fabricadas en el futuro también son analizadas.

Acknowledgements

Primarily, I would like to use this space in order to thank all people who have been involved somehow in this project. My experience and learning process definitely would have not been the same without the advice and guidance of each one of my supervisors. The regular meetings held at both KTH and Ericsson have made this project much easier.

I would also like to thank my family, their continuous support in all aspects, has allowed me to enjoy this unforgettable experience that has not only enriched me professionally but also personally.

To conclude, I want to thank Ericsson for giving me the opportunity to enjoy such a wonderful experience and providing me with everything necessary to make this project possible.

Contents

Acronyms

EM	Electromagnetic
TEM	Transversal Electromagnetic
TE	Transversal Electric
TM	Transversal Magnetic
RWG	Rectangular Waveguide
IoT	Internet of Things
DRWG	Double-Ridged Waveguide
QRWG	Quadruple-Ridged Waveguide
MFEL	Maxwell Fish Eye Lens
HMFEL	Half-Maxwell Fish Eye Lens
PDM	Polarization-Division Multiplexing
IBZ	Irreducible Brillouin Zone

List of Figures

Chapter 1

Introduction

5G is the name given to the next generation of mobile communications networks, the arrival of this technology is expected to bring many improvements and change the way in which people interact with each other. Some of these enhancements are: a huge increase in the network capacity, up to 100 times faster data rates compared to 4G in order to approach the constantly growing demand for data traffic; the latency will be considerably reduced to 1-10 ms, enabling some new services such as the remote control of vehicles and medical procedures; and network slicing, which is the possibility of creating multiple logical networks, each dedicated to a specific service. All these improvements could also enable the connection of a massive number of devices, having a positive impact on the development of the technology known as Internet of Things (IoT). [1]

However, the arrival of this new technology will not come alone but will also bring some new requirements. The main idea in 5G is to move to higher frequencies, much less overloaded and able to provide higher data rates. The latter is the reason why mmWave bands, with frequencies ranging from around 30 to 300 GHz, has gained such importance in recent years. As the frequency increases, so does the free space losses. Due to the latter, old devices such as antennas designed to operate at lower frequencies will need to be replaced. These new devices will have counteract this effect, for instance, by increasing the directivity. Moreover, 5G antennas could also need to fulfill with some other requirements such as the ability to reconfigure their radiation pattern and being low losses in order to reduce the power consumption.

Some options such as arrays have been previously analyzed. However, the losses of their feeding networks is high at these frequencies. Others such as reflector antennas show difficulties to produce electronically steerable radiation beams. [2–5]

Lenses have been used for many different purposes, from the most popular application in glasses in order to correct the aberrations of the lens in the eye to their use in devices such as cameras and microscopes. The working principle of lenses is based on refraction, which is the property that defines the change in the direction of rays as they cross the boundary between two different media. This property makes lenses able to be used in the design of devices such as antennas. In transmission, by placing a source in the focal point, a spherical wave can be transformed into a planar wave. On the other hand, in reception, the fields coming from different directions can be focused in a single point. Therefore, increasing considerably the directivity on both cases. However, there were two main reasons why lens antennas were not very popular before the arrival of 5G: first, the size of the wavelength at low frequencies made lenses bulky; and second, they were expensive to be manufactured.

Lens antennas are considered a type of aperture antennas where the lens is placed in front of the feed in order to modify the fields. A waveguide has been usually used as the source in lens antennas. Depending on the orientation of the electric field inside the waveguide, the wave is said to have a certain polarization. By using PDM, the communication would become more efficient since it would mean that a higher number of channels could be allocated in the same frequency range. The goal of this thesis is the design of a dual-polarized array feed for lens antennas operating in the mmWave spectrum.

This document is organized as follows: Chapter 2 provides an explanation of all the basic concepts used in this project as well as an overview on the state of the art; Chapter 3 describes the design process of both the dual-polarized feed and the Gutman lens; the simulations results for the complete system can be seen in Chapter 4; Chapter 5 shows some prototype ideas to be manufactured in the future; some conclusions and future work lines are stated in Chapter 6.

Chapter 2

Theoretical Background

The main goal of this chapter is to explain some of the main concepts which are used in this project.

2.1 Waveguides

A waveguide is a structure used to transport EM waves, specially microwaves, from one point to another. Waveguides have very low losses and are able to handle very large amounts of power. A waveguide is basically a hollow pipe of metal composed of a single conductor, the metal walls, which enable the propagation of EM waves in the form of modes. The modes are the names given to the different solutions of the Maxwell's equations when the proper boundary conditions are established. Since they only have one conductor, no Transversal Electromagnetic (TEM) mode is supported, and only Transversal Electric (TE) and Transversal Magnetic (TM) modes can propagate. [6, 7].

2.1.1 Rectangular Waveguides

Waveguides can have different shapes depending on their cross-sectional configuration. A Rectangular Waveguide (RWG), see Fig. 2.1.1 is the most common one. A RWG can be analyzed according to its cross-sectional dimensions, the width a (the wider dimension) and height b (the narrower dimension), which determine the cut-off frequency of each mode. A mode excited below its cut-off frequency is strongly

attenuated. Therefore, a waveguide acts as a high-pass filter.

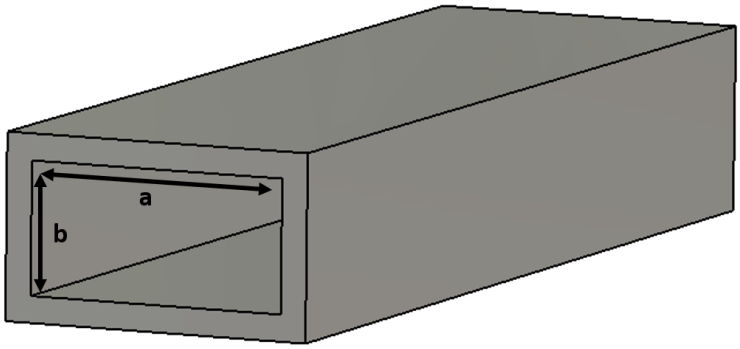

Figure 2.1.1: Rectangular waveguide (RWG)

The TE and TM modes are labelled by using two integer subscripts, n and m, which indicate the number of maxima of the field along the two transverse directions. The TE_{10}, see Fig. 2.1.2, is the fundamental mode in the RWG since it has the lowest cut-off frequency. The colormap represents the intensity of the electric field, where blue is the minimum and red the maximum. The value of the cut-off frequency for the fundamental mode can be calculated by using the following formula

$$f_{c,10} = \frac{c}{2a} \tag{2.1}$$

where c is the constant corresponding to the speed of light in the medium inside the waveguide. In order to avoid dispersion, due to the different velocities at which every mode propagates inside the waveguide, and the complexity that it would generate, the use of the RWG is normally restricted to an operation band. The lower and upper limit are defined by the cut-off frequency of the fundamental mode TE_{10} and the cut-off frequency of the second mode. For the specific case where the height b of the RWG is smaller than half the width a, the cut-off frequency of the second mode TE_{20}, see Fig. 2.1.2, also equals twice the cut-off frequency of the fundamental mode. The latter, is the best value in terms of bandwidth which can be obtained in a RWG.

As previously explained, the main goal of this thesis is to design a dual-polarized feed for lens antennas. In order to achieve that, it is necessary to design a waveguide able

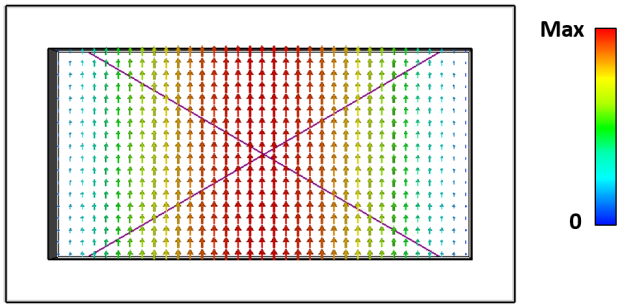

(a)

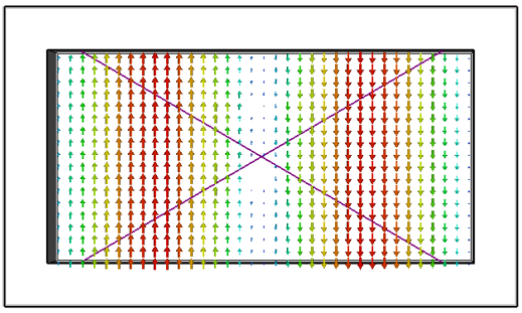

(b)

Figure 2.1.2: First two modes in a RWG: a) TE_{10} and b) TE_{20}

to support the propagation of two orthogonal modes at the same time. By using a waveguide with a square cross-section, it is possible to have two modes, TE_{10} and TE_{01}, see Fig. 2.1.3, with the same cut-off frequency.

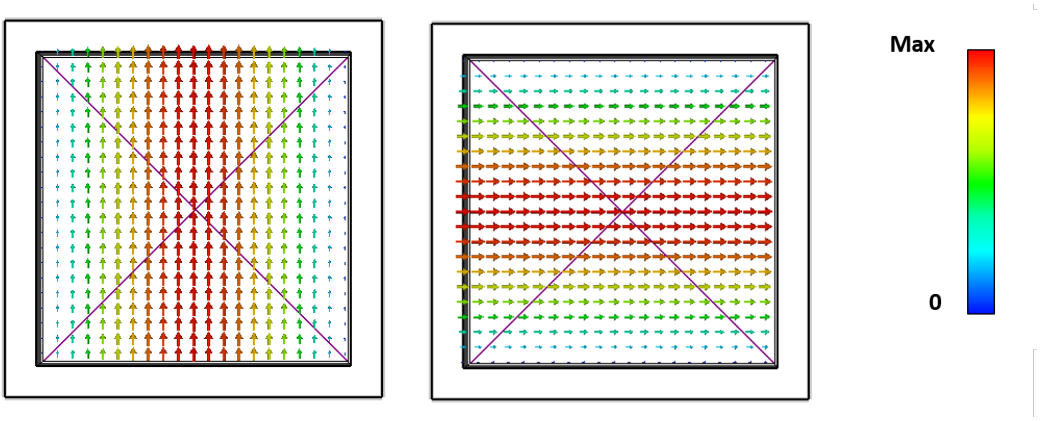

(a) (b)

Figure 2.1.3: Two orthogonal modes in a RWG: a) TE_{10} and b) TE_{01}

2.1.2 Coaxial cable

Once designed a waveguide which can support the propagation of two orthogonal modes, the next step to excite each one of these modes. For that purpose, a coaxial cable, see Fig. 2.1.4, is usually utilized. A coaxial cable is a transmission line consisting of two conductors which might be filled either with vacuum or with a dielectric material in between the inner and the outer conductor. Since coaxial cables have two conductors, it implies that, unlike waveguides, they are able to support a TEM mode and do not have any cut-off frequency.

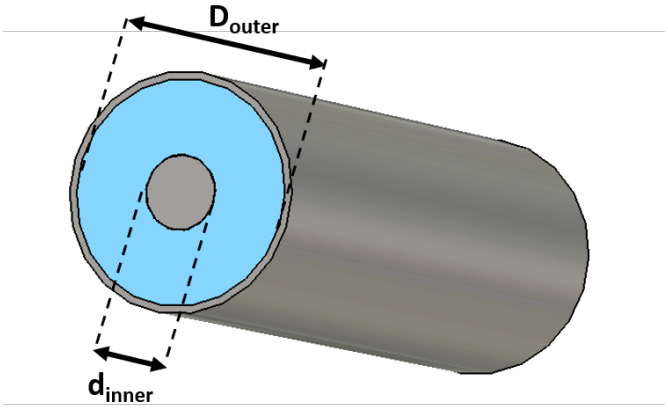

(a)

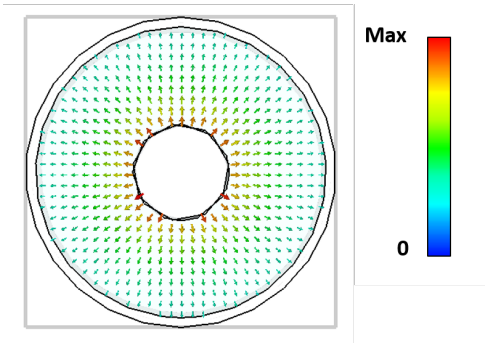

(b)

Figure 2.1.4: a) Coaxial cable and b) TEM mode in a coaxial cable

One of the most important parameters of coaxial cables is the concept of characteristic impedance Z_o, which is the ratio of the amplitudes of voltage and current of a wave propagating along a transmission line without any reflection in the opposite direction.

It can be calculated according to the following equation

$$Z_0 = \frac{138 \log_{10}(\frac{D_{outer}}{d_{inner}})}{\sqrt{\epsilon_r}} \tag{2.2}$$

where D_{outer} is the inner diameter of the outer conductor, d_{inner} is the diameter of the inner conductor and ϵ_r is the relative dielectric constant of the material in between the inner and the outer conductor.

2.1.3 Coaxial-to-Rectangular Waveguide transition

One of the most popular kinds of transitions is known as right-angle transition, see Fig. 2.1.5. In this transition, the inner conductor of the coaxial cable is inserted in the waveguide through one of the metal walls. The two main parameters in this kind of transitions are the gap distance h between the waveguide and the inner conductor of the coaxial cable, and the distance $D_{backshort}$ to the backshort, which is the name given to the metal plate located in the back part of the waveguide in order to reflect back the EM waves propagating in the wrong direction. The value of the latter is usually around a quarter of the wavelength inside the waveguide at the center frequency of the desired operation band. It is done in order to ensure that the waves traveling in the wrong direction and being reflected at the backshort, add in phase with the waves propagating in the right direction. By using that configuration, the vertically oriented coaxial cable would excite the fundamental mode TE_{10} mode inside the RWG. By changing the position of the coaxial cable and orientating it horizontally, the TE_{01} mode would be excited instead.

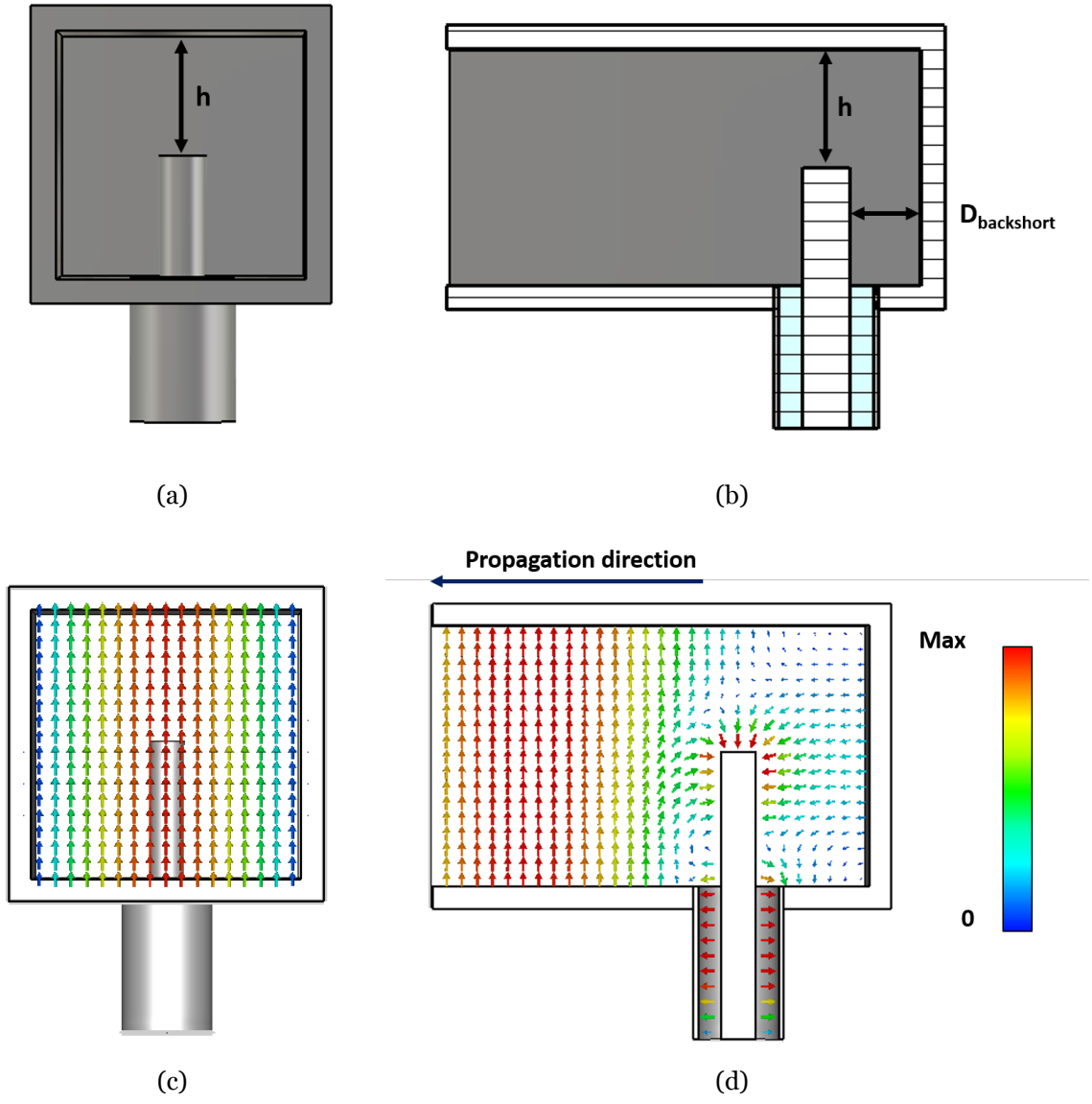

Figure 2.1.5: Right angle Coaxial-to-Rectangular Waveguide transition: a) Front view, b) cross-section side view, c) front view excited TE_{10} and d) cross-section side view excited TE_{10}

2.1.4 Quadruple-Ridged Waveguides

A Double-Ridged Waveguide (DRWG), see Fig. 2.1.6, is similar to a RWG. However, by introducing two ridges in the region of the RWG where the electric field is maximum, the cut-off frequency of the fundamental mode TE_{10} is lowered. This reduction implies that, for the same cut-off frequency of the fundamental mode, a DRWG will have a smaller cross-sectional shape compared to a conventional RWG. Another advantage is the possibility of tuning the impedance of the waveguide by changing the distance between the ridges. The latter is good for impedance matching when designing the transition from a coaxial cable. On the other hand, the main downsides of a DRWG are the reduction in the power handling capability with respect to a conventional RWG and the inability to support dual-polarization. Due to the latter, a DRWG will not be used in this thesis, however, an extensive analysis on this kind of waveguides can be found in [8–10].

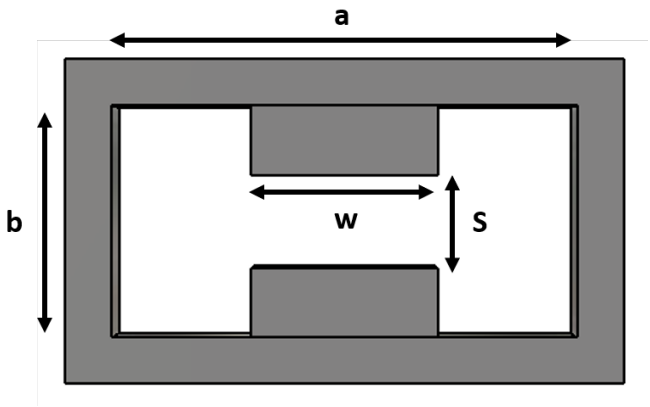

Figure 2.1.6: Double-Ridged Waveguide (DRWG)

Due to their more compact size and lower impedance compared to a conventional RWG along with its capability to support dual-polarization, Quadruple-Ridged Waveguides (QRWGs), see Fig. 2.1.7, are a good choice for the design of dual-polarized feeds. A QRWG has four ridges symmetrically placed in the square cross-section which allow the propagation of the fundamental mode either horizontally or vertically polarized.

The fundamental mode inside a QRWG is the TE_{10}. However, special attention should be paid on the second mode TE_{11} since, unlike what happens in DRWG, the smaller the distance *s* between the ridges, the lower the cut-off frequency of this mode. Due to the latter, the fundamental mode inside a QRWG has a cut-off frequency very close to that

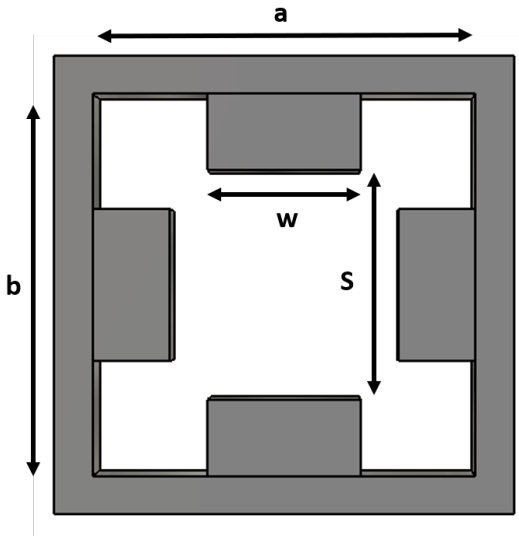

Figure 2.1.7: Quadruple-ridged waveguide

of the second lowest mode. The third mode inside a QRWG is the TE_{20L} and its cut-off frequency is around six times higher than the cut-off frequency of the fundamental mode, which means that, if the excitation of the second lowest mode is suppressed, an operation bandwidth of up to 6:1 can be obtained. In Fig. 2.1.8, can be seen the representation of the electric field for the first three modes in a QRWG. It is also very common to see designs where the corners of the ridges have been cut so that it is possible to further reduce the distance between the ridges and still prevent them from touching each other. [11, 12]

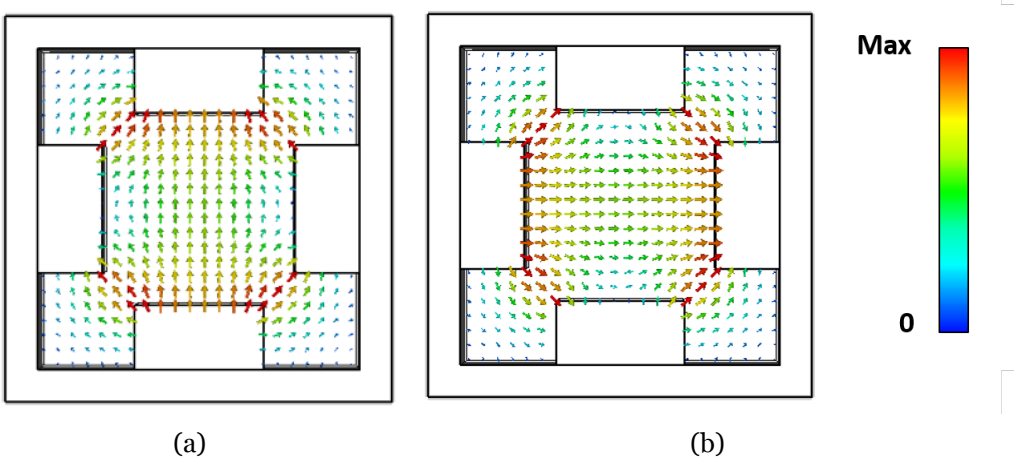

(a) (b)

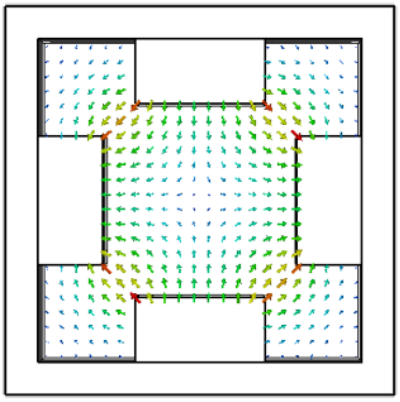

(c)

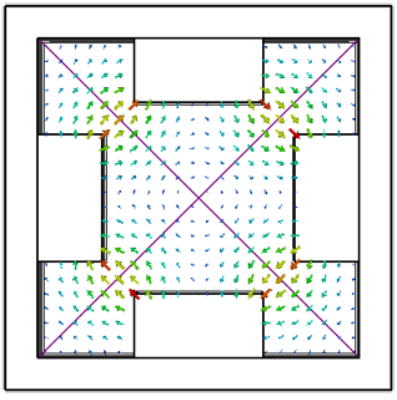

(d)

Figure 2.1.8: First modes in a QRWG: a) TE_{10}, b) TE_{01}, c) TE_{11} and d) TE_{20L}

2.1.5 Coaxial-to-Quadruple Ridged Waveguide transition

In the same way than for a conventional RWG, a coaxial cable can be used in order to excite the desired modes inside a QRWG, see Fig. 2.1.9. In this figure, two coaxial connectors are used, one for the vertical and another one for the horizontal polarization. The inner conductors of the coaxial cables are inserted through the air-holes inside the ridges, creating a coaxial air-line, and connected to the opposite ridges. The radius $r_{air\ gap}$ is designed so that the characteristic impedance of the coaxial air-line is similar to the one of the coaxial cable, thus reducing the reflections. The inner conductor of the coaxial cables are separated by a distance d_{coax}. It is also common to include a cavity in the back part of the QRWG in order to reduce the reflections of the coaxial-to-QRWG transition.

This transition has already been used previously, mainly for the design of dual-polarized horn antennas such as the one shown in [13].

As it has been explained previously, special attention must be paid on this transition in order to excite the desired mode due to the similar value of the cut-off frequency for the first two modes.

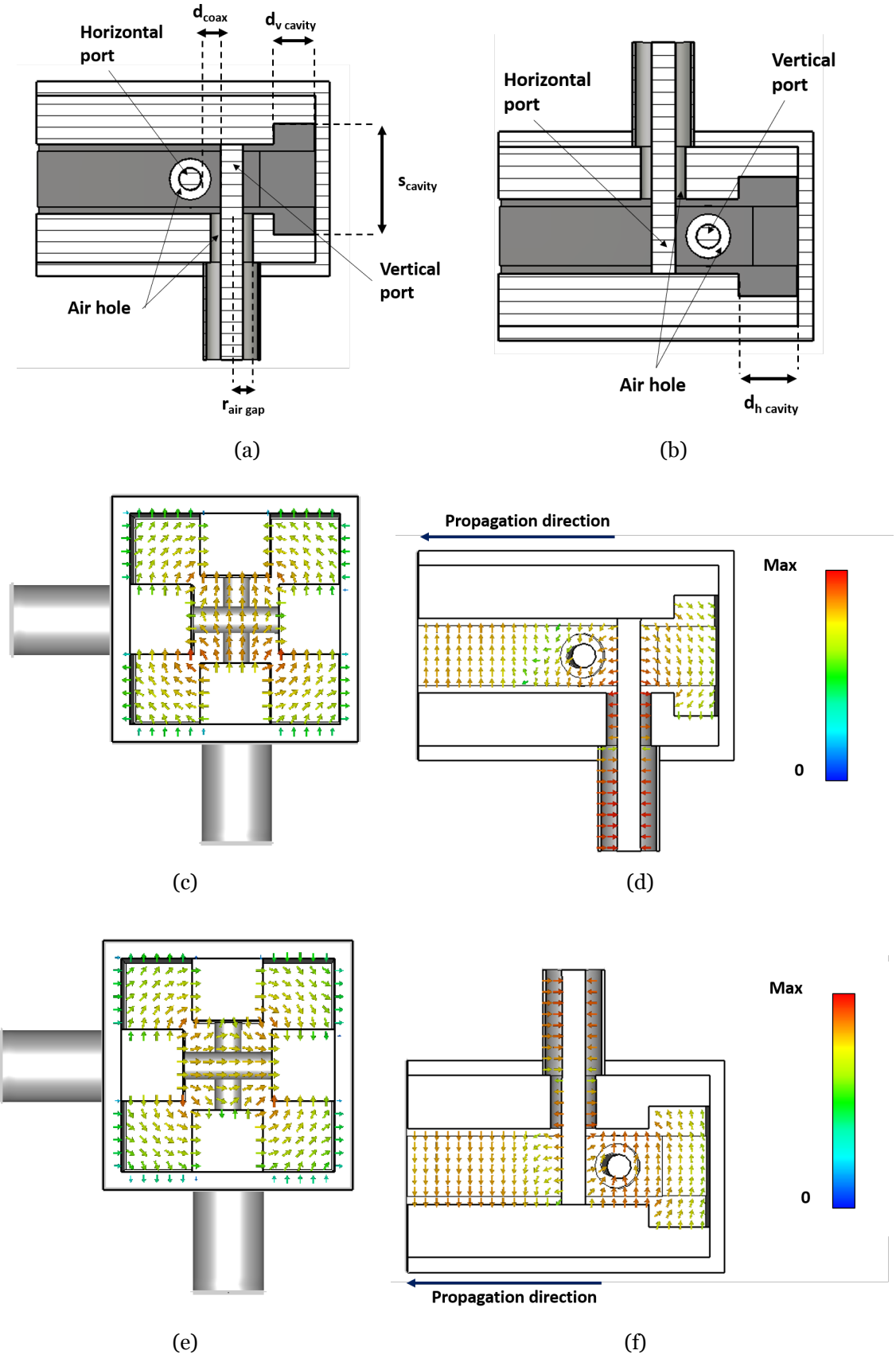

Figure 2.1.9: Right angle Coaxial-to-QRWG transition: a) Front view, b) cross-section side view, c) front view excited TE_{10}, d) cross-section side view excited TE_{10}, e) front view excited TE_{01} and f) cross-section top view excited TE_{01}

2.2 Lenses

As it has been explained previously, lens antennas are a specific case of aperture antennas where the lens is placed in front of the aperture of the source in order to modify the fields. The working principle of a basic lens antenna is shown in Fig. 2.2.1. It can be seen how the convex lens modify the rays coming from the emitter, placed at the focal point, and focus them in a specific direction.

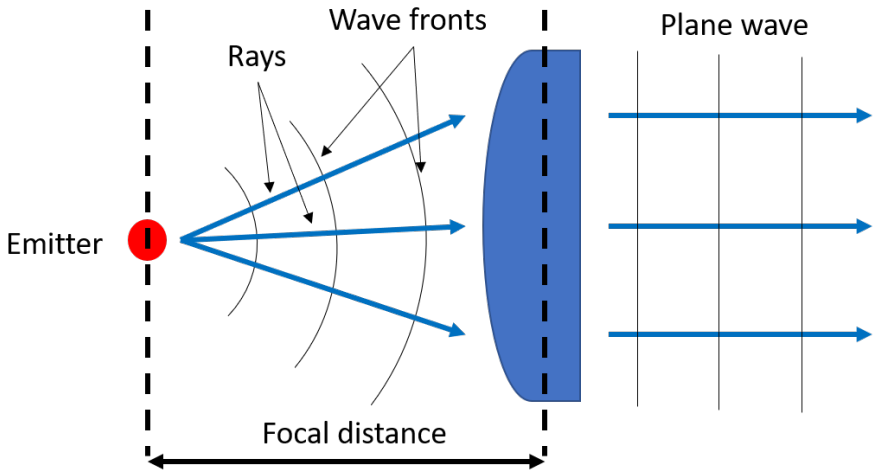

Figure 2.2.1: Working principle of a convex lens antenna

2.2.1 Geometrical optics

Geometrical optics is a model of optics used in order to explain the propagation of waves in terms of rays. A ray is a line perpendicular to a series of consecutive waves. In this model, the ray path can be determined based on the following laws [14]:

- **Refraction:** The change in the direction of rays is due to the phenomenon known as refraction, which is produced when a wave passes from a medium to another with different properties. The change in the direction of the rays can be modeled by using the Snell's law shown below

$$\frac{\sin\theta_1}{\sin\theta_2} = \frac{v_2}{v_1} = \frac{n_1}{n_2} \tag{2.3}$$

where θ is the angle measured from the normal of the boundary, v corresponds to the velocity of the wave in the medium and n is the refractive index of the

medium. A representation of a refracted ray crossing the boundary between two different media can be seen in Fig. 2.2.2.

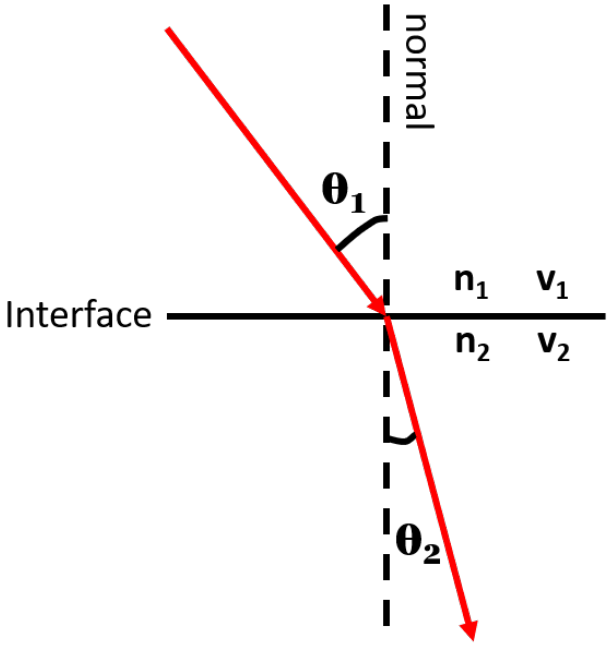

Figure 2.2.2: Refracted ray

- **Reflection:** When a wave crosses the boundary between two different media, some power will be reflected due to the different value of the wave impedance. This phenomenon must be taken into account when designing a lens. A large difference between the wave impedance of air and the wave impedance in the lens would cause a high amount of reflections. Due to the latter, the efficiency of the antenna, the ratio of the power radiated by the antenna to the power delivered to the antenna, would be considerably reduced.

The concept of Fermat's principle can be used in order to explain the behaviour of rays when they propagate in a gradient index medium, where the value of the refractive index continuously changes with position. According to this principle, the path taken by a ray in order to go from one point x_1 to another point x_2 will be the fastest one between these two points. The optical length of this path, L can be determined by using the following equation

$$L = \int_{x_1}^{x_2} n(s)ds \tag{2.4}$$

where $n(s)$ is the value of the refractive index and s is the arc length of the curve [15].

2.2.2 Types of lenses

Lenses can be divided in two main types:

- **Homogeneous lenses**: These lenses are made of a homogeneous material. They can also be divided into two other categories according to their shape: spherical lenses such as the bi-convex; planar-convex; seen in Fig. 2.2.1, bi-concave; planar concave and meniscus lenses, and non spherical lenses such as the elliptical, hyper-hemispherical, hyperbolic and Fresnel lenses. The main limitation of this kind of lenses is the high amount of reflections at the border since the wave impedance in the lens is different from the wave impedance in the air.
- **Gradient index lenses**: These lenses have a space-varying refractive index and, as a consequence of that, it is possible to have a smooth transition from the lower value of the refractive index corresponding to air to the higher one, thus reducing the amount of reflections. Some examples of this kind of lenses are the Luneberg lens [16], the Maxwell Fish Eye Lens (MFEL) [17], the Half-Maxwell Fish Eye Lens (HMFEL) [18] and the Gutman lens [19].

2.2.3 Design techniques

Nowadays, the two most innovative techniques for the design of lenses are [3]:

- **Transformation optics**: This technique was first introduced in the 2000s. It is used in order to explain the change in the space coordinates of a propagating wave as a function of the electromagnetic properties, such as permittivity and permeability, of a specific medium. The latter means that a wave could propagate in the same way in two media with different shapes and electromagnetic properties. This technique can be used in order to create optical devices. This is done by solving an inverse electromagnetic problem where it is necessary to

find the material properties which provide the desired pattern of light. However, this technique is not easy to implement since it is often necessary the use of anisotropic, magnetic and exotic (e.g. sub-unity index) materials with a narrow bandwidth and high losses. The solution is to use approximate solutions such as quasi-conformal mapping. Fully dielectric materials can be used to build these lenses. A discretization process would be necessary in order build gradient index lenses. Moreover, thanks to the continuous development of techniques such as 3D-printing, the manufacturing of these kind of lenses has become easier [20, 21].

- **Metasurfaces**: Metamaterials is the name given to sub-wavelength metallic or dielectric structures with a certain periodicity in three dimensions. These materials are able to provide properties which are not readily obtained in nature. Some of this properties include the ability to produce negative refractive-indexes or manipulate the wave propagation. Metasurfaces are thin metamaterial layers which can be used, for example, in order to guide waves in a 2D configuration. Unlike 3D metamaterials, metasurfaces can be easily manufactured. It enables the possibility of creating fulling metallic lenses which have lower losses than dielectric materials at high frequencies. The main downside of this kind of lenses is that they are limited in bandwidth. However, this aspect can be improved by using the concept of higher symmetries such as twist and glide. [22, 23]

2.2.4 3D printing

In the past, the manufacturing of lenses, specially gradient index lenses, was quite difficult due to the lack of techniques which enabled the possibility to model this space-varying refractive index. However, with the emergence of new additive manufacturing techniques such as 3D printing it has become much easier to change the material properties depending on the position. Since several values of the refractive index are needed and due to the lack of dielectric materials commercially available, a technique consisting in changing the amount of material deposited in a small volume of the lens can be utilized in order to obtain different effective permittivities.

2.2.5 Gutman lens

A Gutman lens is a rotationally-symmetric gradient index lens where a spherical wave is transformed into a pseudo-planar wave. This property makes a Gutman lens a good candidate for multi-beam and beam scanning antenna applications. In this kind of lenses, the focal point is located on a sphere with a smaller radius than the lens. One advantage of this kind of lenses is its polarisation independence. The refractive index of a Gutman lens can be calculated as follows [24]

$$n(r) = \sqrt{\frac{1 + (f/R)^2) - (r/R)^2}{(f/R)^2}} \tag{2.5}$$

where f is the radius of the sphere where the focal point is located, R is the radius of the lens and r is the radial position. An example of an additive manufactured Gutman lens can be seen in Fig. 2.2.3.

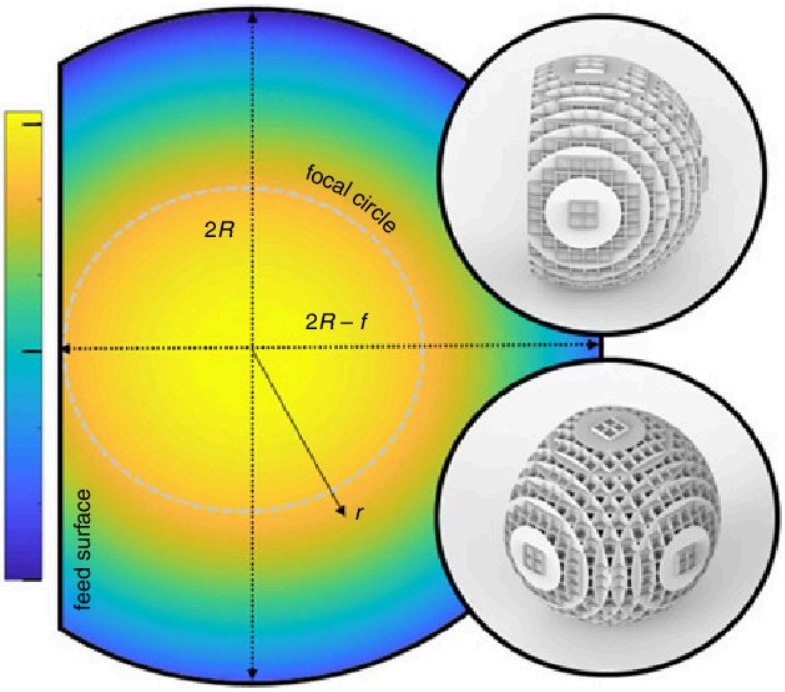

Figure 2.2.3: Cross-sectional colour map of the refractive index in a Gutman lens where the radius of the focal point is half the radius of the lens. The two small pictures are 3D models of the final design ready to be printed. [24]

Chapter 3

Design of the Dual-Polarized Lens Antenna

The aim of this chapter is to explain the design process of the dual-polarized lens antenna. As it has been explained previously, the main goal of this thesis is to design a dual-polarized feed which can be utilised as a source for lens antennas in the future 5G communication systems. However, it is necessary to clarify some of the requirements which have to be taken into account in the design:

- The lens antenna must operate at the frequency band of 28 GHz with around 10% bandwidth
- The dual-polarized feed must be suitable to be used in arrays
- The feed must be as small as possible in order to have a high beam cross-over level

3.1 Dual-polarized feed

The design of the dual-polarized feed can be divided into two different parts, each of them explained in a different section. Section 3.1.1 explains the steps followed in order to design a first version of the dual-polarized feed based on a QRWG. Section 3.1.2 shows the final design of the dual-polarized feed with some changes with respect to the first design.

3.1.1 First design

A QRWG is the structure chosen for the design of the dual-polarized feed. The size of the QRWG was chosen to be 5 mm so that it was smaller than a conventional RWG operating at 28 GHz. It must be noted how the cut-off frequency of a conventional RWG with these cross-sectional dimensions would be around 30 GHz, which is above the desired frequency band of operation. However, in a QRWG, the cut-off frequency is reduced due to the ridges, thus making this size suitable for the design.

Once chosen the structure and its cross-sectional dimensions, the following step is to design the transition from both coaxial connectors to the QRWG in order to excite the different polarizations. The main problem with the transition shown in Fig. 2.1.9 is that the disposition of the connectors makes this design not suitable to be used in an array since it would not be possible to put several feeds next to each other without any gap in between, thus deteriorating considerably the scanning. The changes introduced in the traditional transition consist basically in creating a pin which is attached to the ridge and extends to the opposite ridge where it is introduced through a cavity. Then, a cylindrical air-cavity is created by taking advantage of the space between the ridges of two contiguous QRWGs in such a way that the inner conductor of the coaxial cable connected on the back part of the QRWG can touch the pin in order to excite a specific polarization inside the QRWG as can be seen in Fig. 3.1.1

The next step is to design the ridges of the QRWG, see Fig. 3.1.1, so that the input impedance of the QRWG is as close as possible to 50 Ohms, which is the characteristic impedance of the coaxial cable, in order to achieve a good impedance matching at 28 GHz. It can also be seen how the edges of the ridges are cut so that the ridges can be even closer and still prevent them from touching each other.

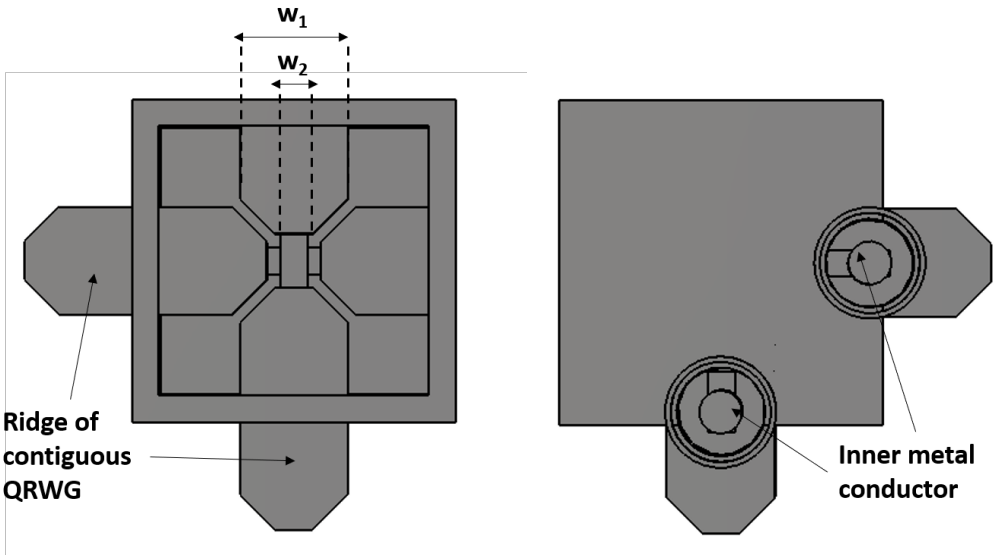

(a) (b)

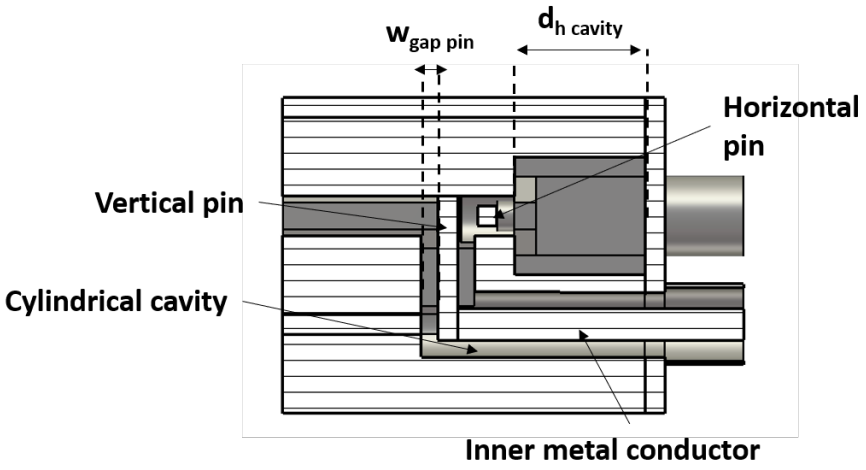

(c)

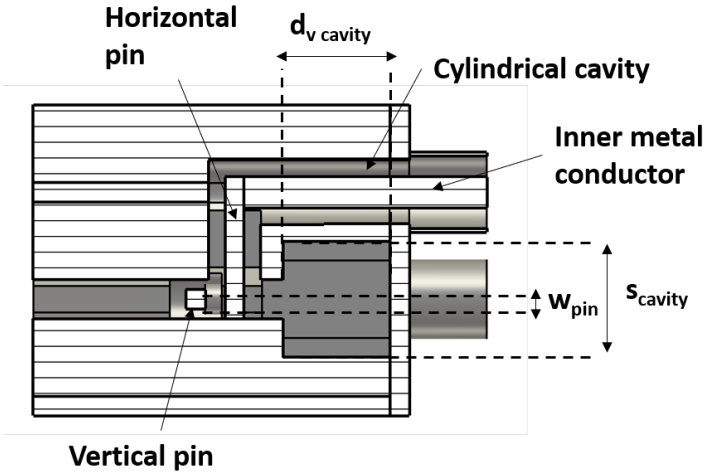

(d)

Figure 3.1.1: Coaxial-to-QRWG transition with both coaxial connectors on the back part of the QRWG. a) Front view, b) back view, c) cross-section side view and d) cross-section top view

Once chosen the dimension of the ridges, a simulation is run in order to obtain the value of the cut-off frequencies, see Fig. 3.1.2 for the first modes inside the designed QRWG. The results show how the cut-off frequency of the TE_{11} mode is very similar to the one of the fundamental mode.

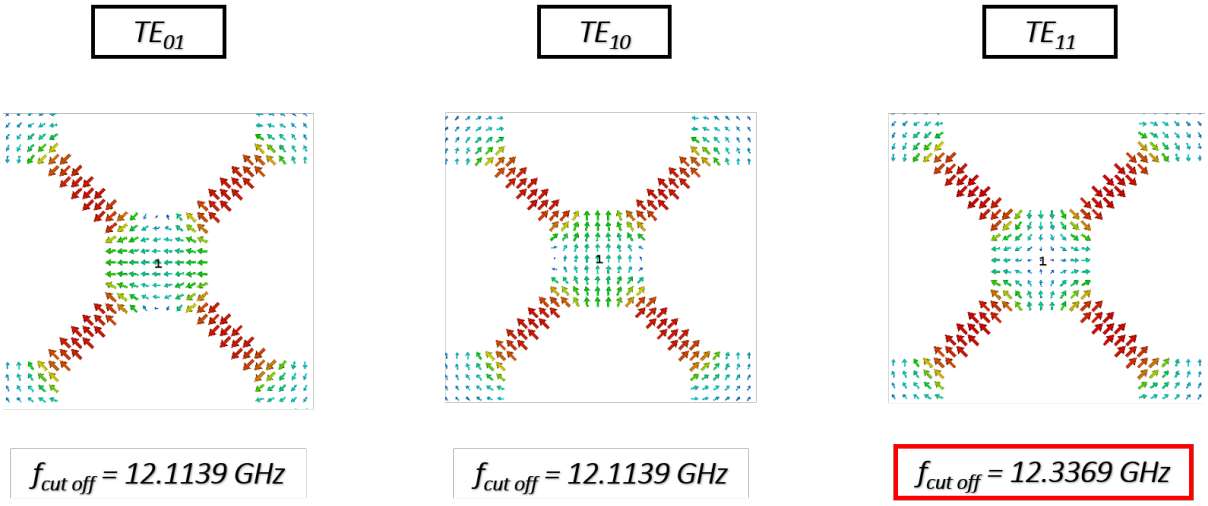

Figure 3.1.2: Cut-off frequencies for the first modes inside the designed QRWG

The results for the S-parameters of the coaxial-to-QRWG transition can be seen in Fig. 3.1.3. Notice that these results do not take into account the reflections at the end of the QRWG when radiating to free space and a QRWG with an infinite length is considered instead.

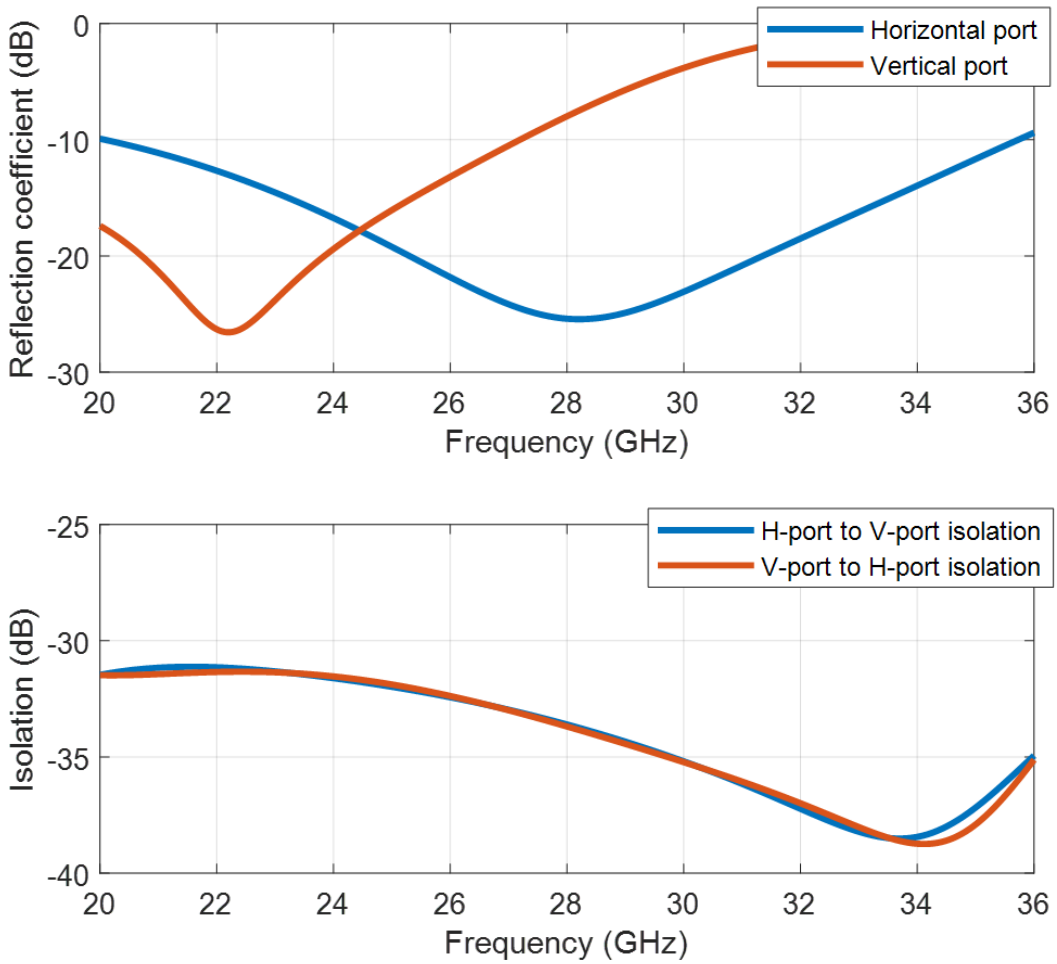

Figure 3.1.3: S-parameters results of the coaxial-to-QRWG transition for the first design of the dual-polarized feed. The dimensions are $d_{backshort\,H-port} = 3.75mm$, $d_{coax} = 0.5mm$, $w_{pin} = 0.5mm$, $s = 1mm$, $w_1 = 2mm$, $w_2 = 0.7mm$, $d_{inner} = 0.8mm$, $D_{outer} = 1.85mm$, $r_{air\,gap} = 0.825mm$, $w_{gap\,pin} = 0.425mm$, $a = 5mm$, $s_{cavity} = 3mm$, $d_{h\,cavity} = 2.75mm$, $d_{v\,cavity} = 3.3mm$

The results show how the horizontal port, the one whose pin is close to the backshort of the QRWG, has the resonance frequency centered at 28 GHz. However, the vertical port has its resonance peak at a lower frequency due to the fact that the vertical pin is further away from the backshort. Moreover, it can be also seen how the isolation between the two ports is quite good. Therefore, it is necessary to introduce a change in the structure in such a way that it is possible to move that peak higher in frequency while keeping the resonance peak of the horizontal port at the same position. For that purpose, a metal pin, see Fig. 3.1.4, is introduced in between the vertical ridges in the backshort cavity in order to reduce the distance from the vertical pin to the backshort without affecting the distance from the horizontal pin to the backshort.

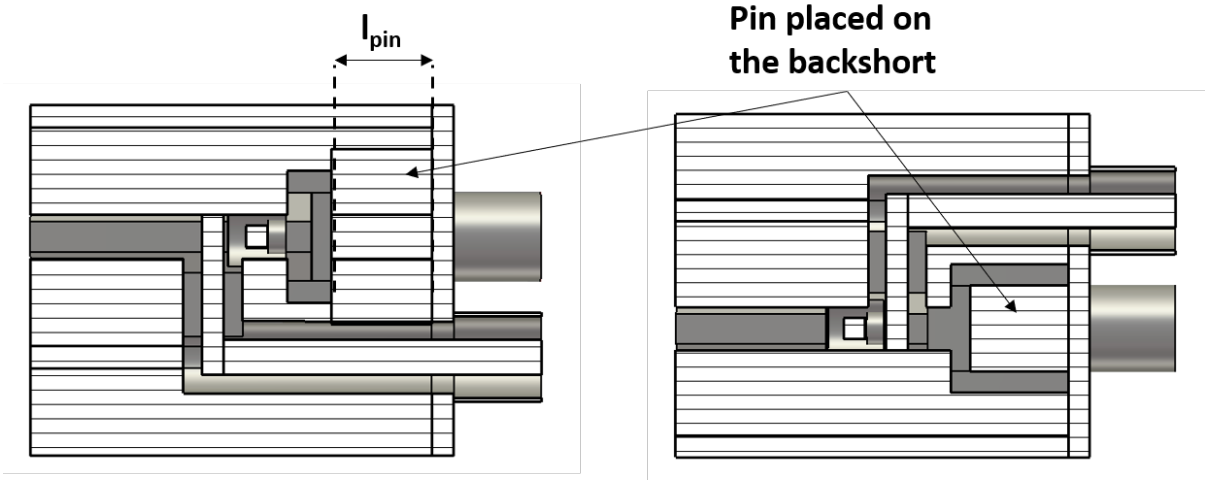

Figure 3.1.4: Coaxial-to-QRWG transition showing the pin introduced in the backshort. Cross-section side view on the left and cross-section top view on the right

The S-parameters for coaxial-to-QRWG with the modified backshort cavity including the pin can be seen in Fig. 3.1.5. It can be seen how the resonance peak of both ports is at the center frequency now, thus achieving good impedance matching in the coaxial-to-QRWG transition. Notice that these results do not take into account the reflections at the end of the QRWG when radiating to free space and a QRWG with an infinite length is considered instead.

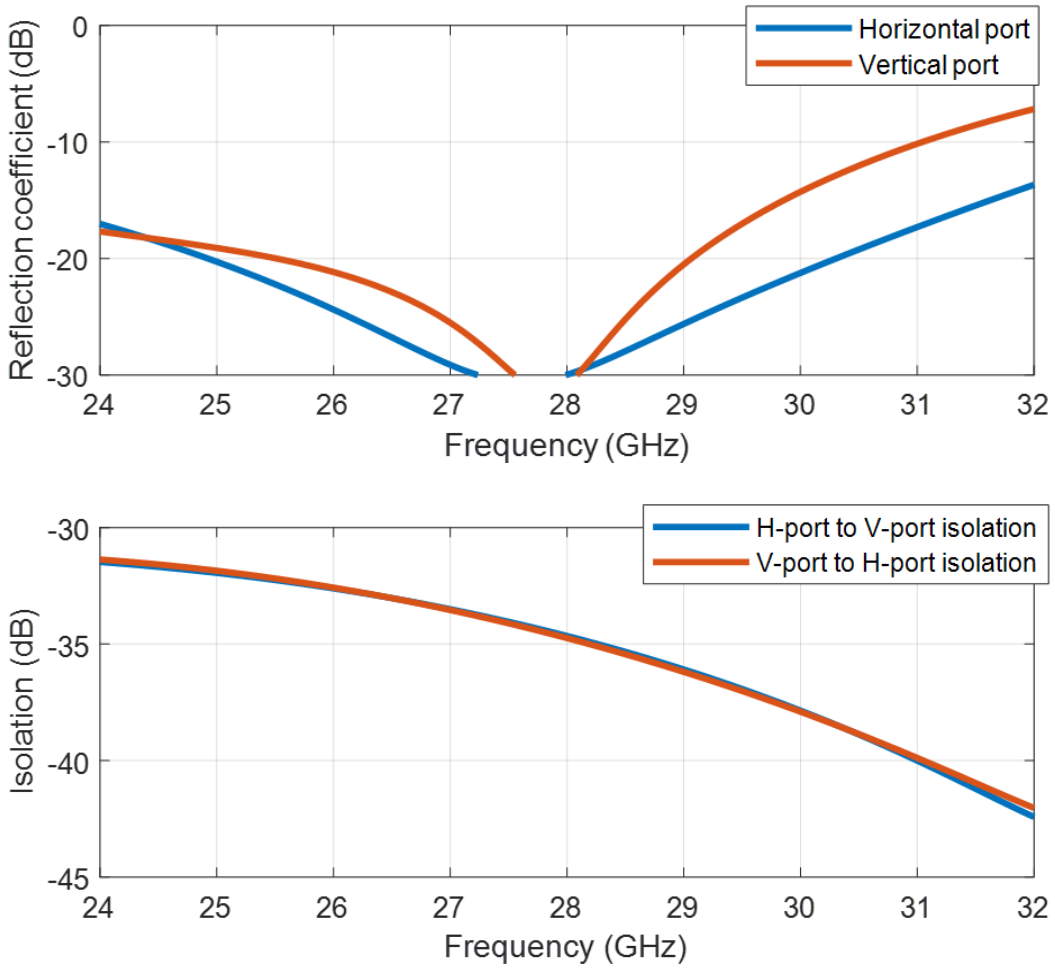

Figure 3.1.5: S-parameters results of the coaxial-to-QRWG transition with modified backshort cavity including the pin. The dimensions are $d_{backshort\,H-port} = 3.75mm$, $d_{coax} = 0.5mm$, $w_{pin} = 0.5mm$, $s = 1mm$, $w_1 = 2mm$, $w_2 = 0.7mm$, $d_{inner} = 0.8mm$, $D_{outer} = 1.85mm$, $r_{air\,gap} = 0.825mm$, $w_{gap\,pin} = 0.425mm$, $a = 5mm$, $s_{cavity} = 3mm$, $d_{h\,cavity} = 2.75mm$, $d_{v\,cavity} = 3.3mm$, $l_{pin} = 2.3mm$

Once designed the transition from both coaxial cables to the QRWG , it is time to evaluate the performance of the dual-polarized feed when radiating to free space. However, before that, some changes have to be made to the current feed in order to reduce the reflections when radiating to free space. Until now, the distance between the ridges has been kept very small in order to lower the impedance of the QRWG and make it as similar as possible to the impedance of the coaxial connector. The main goal now is to increase this distance at the end of the QRWG in order to have a higher value of the wave impedance and create a smooth transition to the impedance in free space as can be seen in Fig. 3.1.6. Notice how the ridges can not be completely removed at the end of the QRWG, otherwise the cut-off frequency would be above the required frequency band of operation.

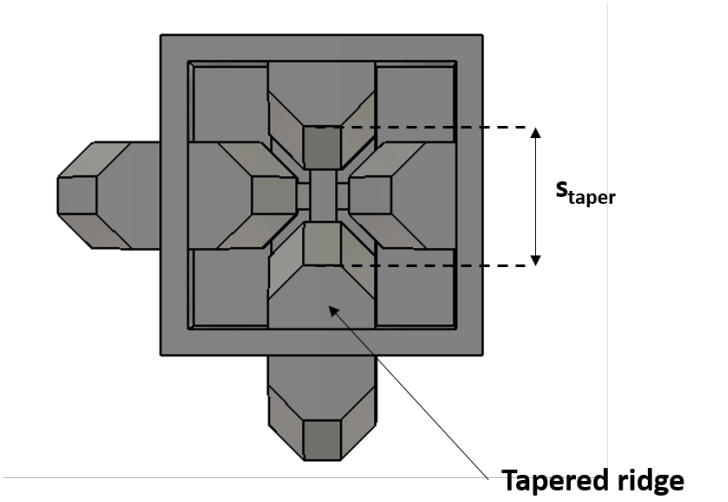

(a)

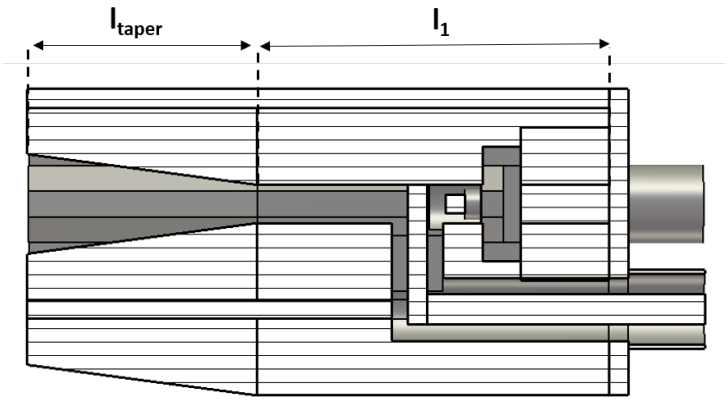

(b)

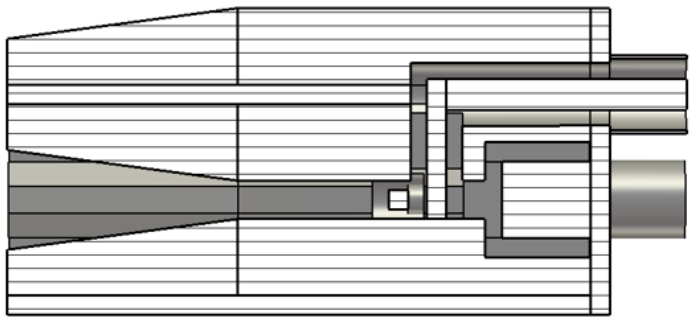

(c)

Figure 3.1.6: QRWG with tapered ridges: a) Front view, b) side cross-section and c) top cross-section.

The S-parameters for the dual polarized feed when radiating to free space can be seen in Fig. 3.1.7. It can be noticed in the results how not only both ports have a good matching from around 27 to 30 GHz but also the isolation between them is still quite good when radiating to free space.

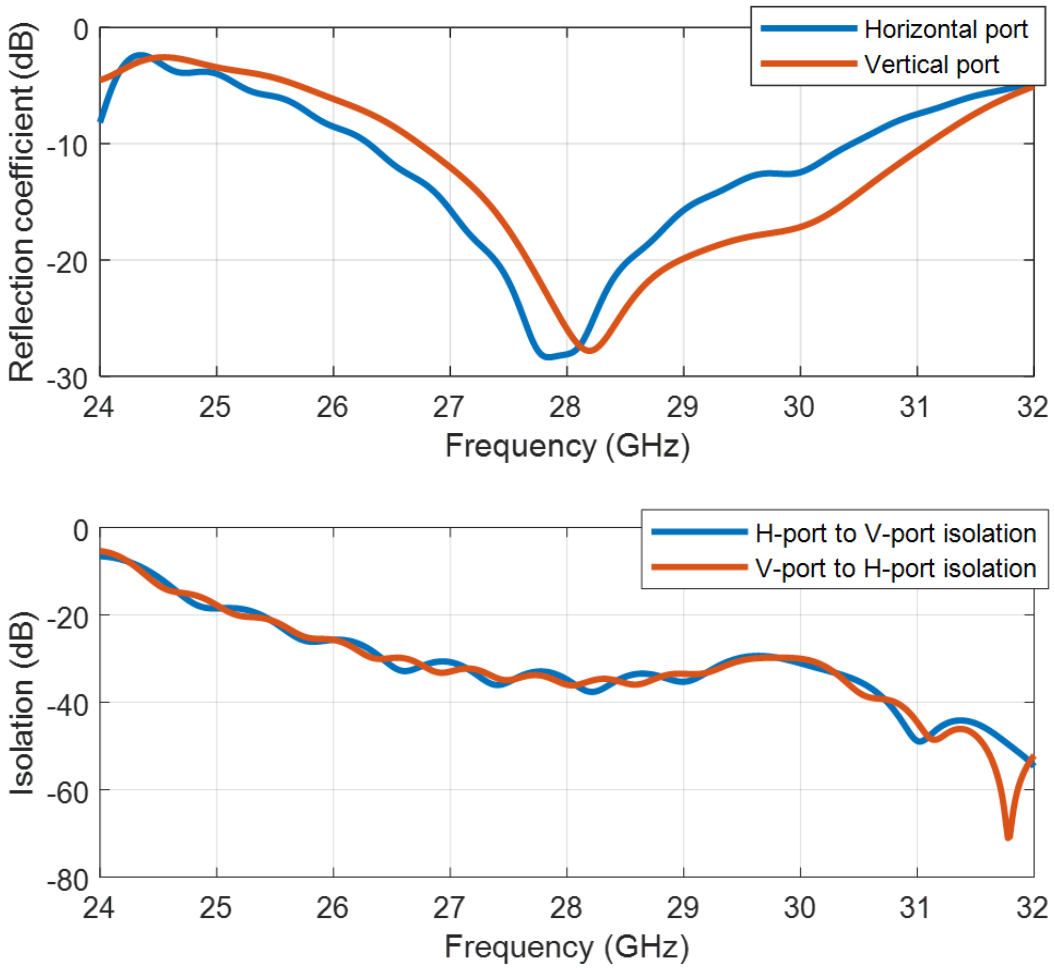

Figure 3.1.7: Results of the S-parameters for the first design of the dual-polarized feed when radiating to free space. The dimensions are $d_{backshort\,H-port} = 3.75mm$, $d_{coax} = 0.5mm$, $w_{pin} = 0.5mm$, $s = 1mm$, $w_1 = 2mm$, $w_2 = 0.7mm$, $d_{inner} = 0.8mm$, $D_{outer} = 1.85mm$, $r_{air\,gap} = 0.825mm$, $w_{gap\,pin} = 0.425mm$, $a = 5mm$, $s_{cavity} = 3mm$, $d_{h\,cavity} = 2.75mm$, $d_{v\,cavity} = 3.3mm$, $l_{pin} = 2.3mm$, $l_1 = 9.175mm$, $l_{taper} = 6mm$, $s_{taper} = 2.6mm$

The next step is to check the far field results of the designed dual-polarized feed. The 3D radiation pattern of the dual-polarized feed can be seen in Fig. 3.1.8

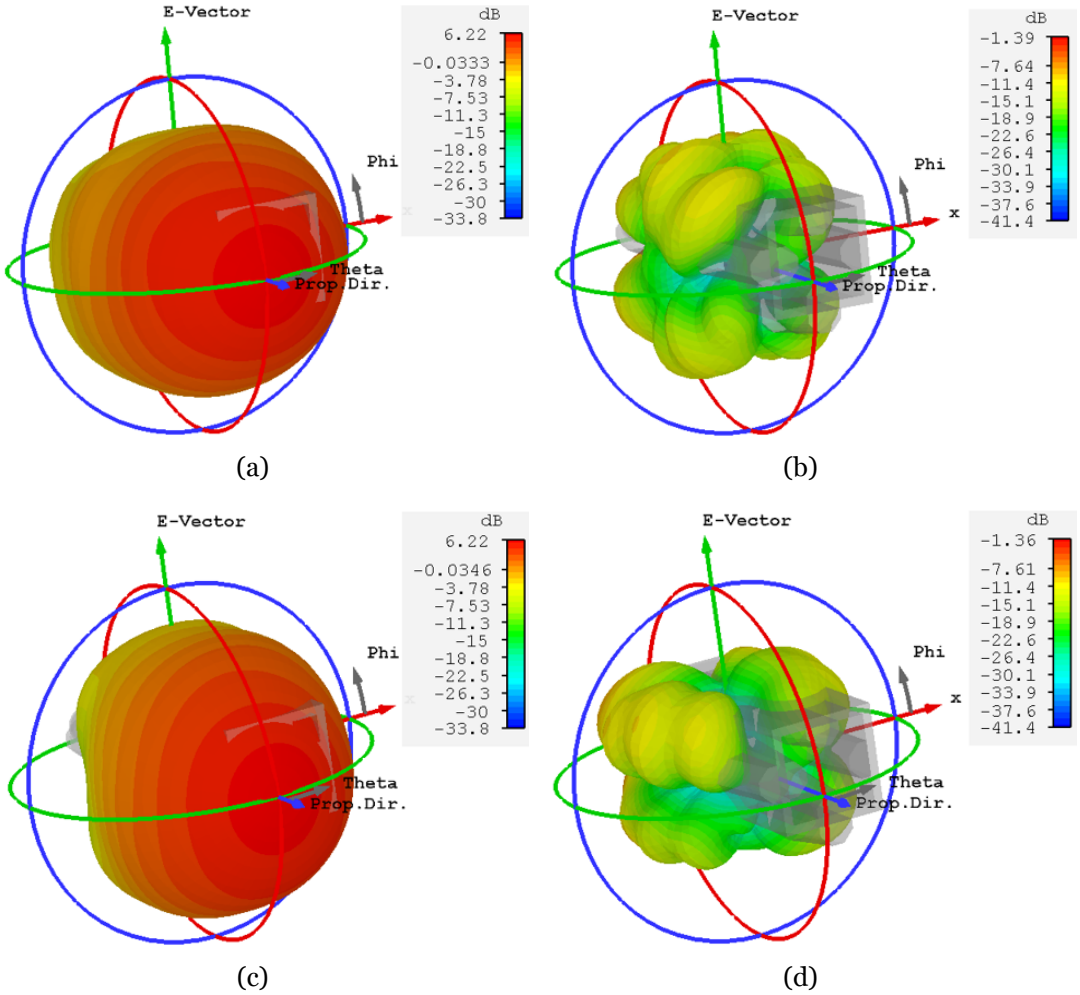

Figure 3.1.8: 3D radiation pattern of the first design of the dual-polarized feed at 28 GHz: a) Co-Pol horizontal port, b) cross-Pol horizontal port, c) co-Pol vertical port and d) cross-Pol vertical port

It can be noticed in the picture above how there are four beams in the radiation pattern of the cross-polarization. These four beams in the cross-polarization are due to the fact that the electric field at the aperture of the dual-polarized feed is not completely vertical or horizontal. Due to the presence of ridges at the aperture, there are some fields which are oriented at 45° between the ridges, see Fig. 3.1.9 and are creating those four beams in the cross-polarization.

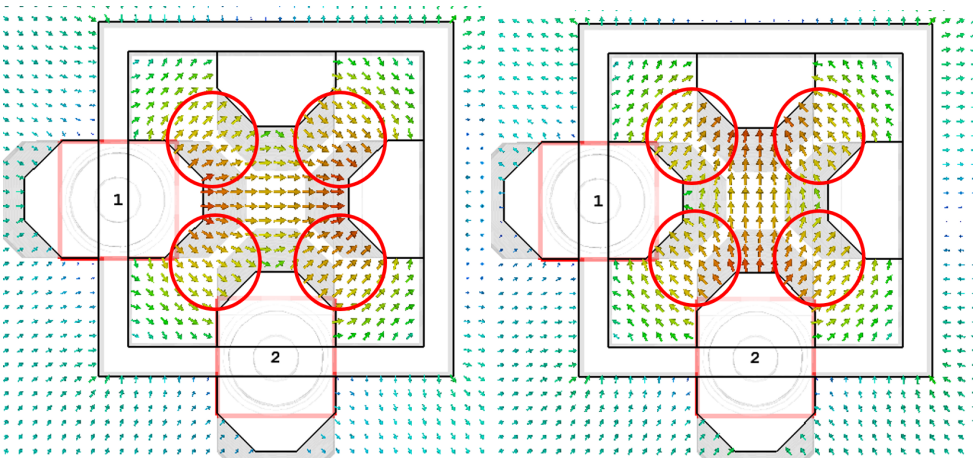

(a) (b)

Figure 3.1.9: Electric field at the aperture of the dual-polarized feed. The fields between the ridges (circled in red) are responsible of the beams in the radiation pattern of the cross-polarization: a) Horizontal port and b) vertical port

In Fig. 3.1.10, it can be seen a 2D representation of the radiation pattern for different frequencies. In this figure, the value of ϕ is kept constant at 45°in order to show the main peaks of the cross-polarization.

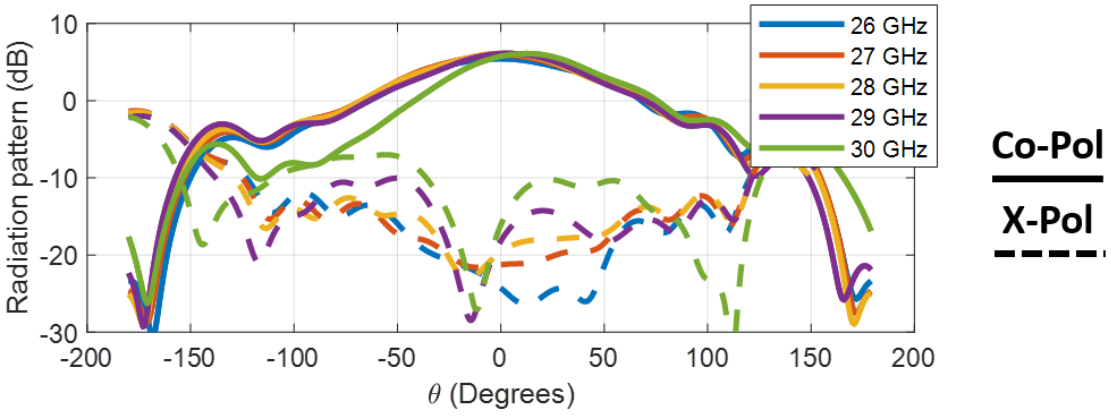

(a)

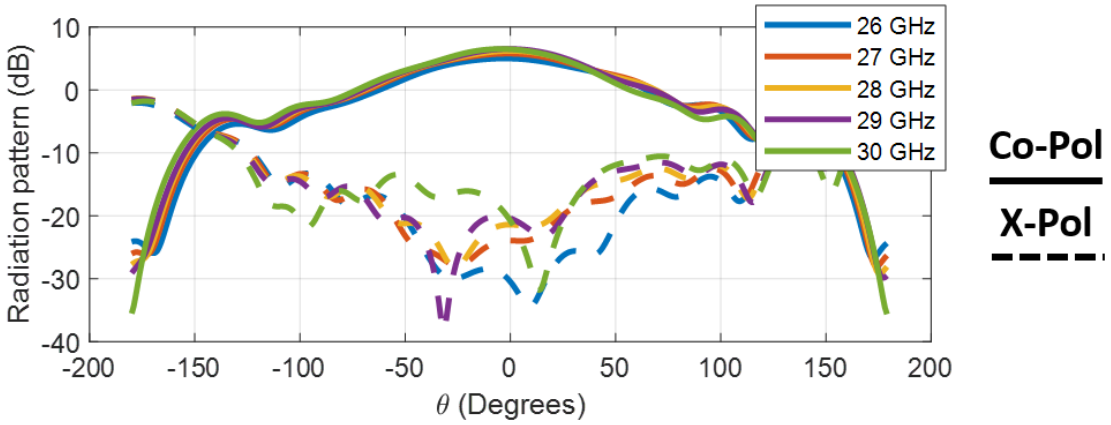

(b)

Figure 3.1.10: 2D representation of the radiation pattern for the first design of the dual-polarized feed at 28 GHz ($\phi = 45°$): a) Horizontal port and b) Vertical port

It can be shown in the picture above how the radiation pattern of both the co-polarization and cross-polarization are worse at 30 GHz, specially for the horizontal port. In order to understand these results, it is necessary to see the electric field at that frequency as can be seen in Fig. 3.1.11

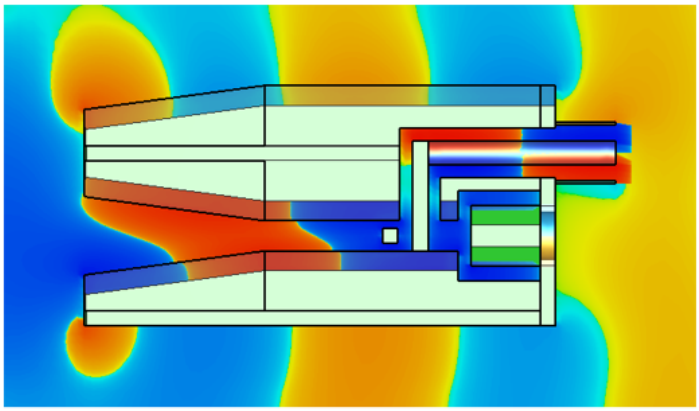

(a)

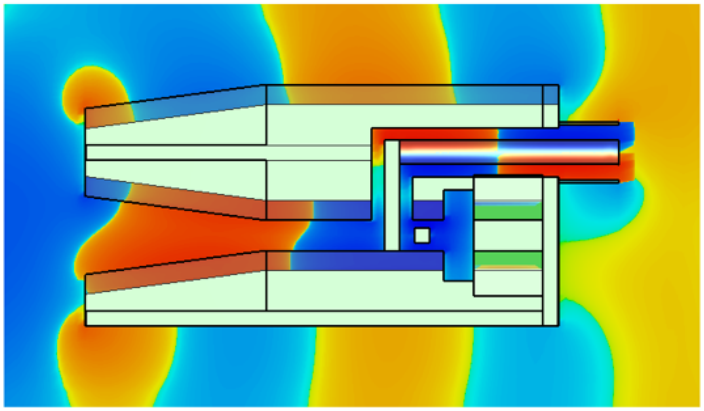

(b)

Figure 3.1.11: a) Cross-section top view electric field horizontal port. b) Cross-section side view electric field vertical port

It can be noticed in the picture above how the electric field inside the waveguide is not very uniform at 30 GHz, and it is worse for the horizontal port than for the vertical port, which explains the results shown in Fig. 3.1.10. The main reason why it is happening is because the two pins inside the waveguide are not only exciting the fundamental mode but also the higher order mode TE_{11} as was explained in the introduction.

3.1.2 Final design

The previous subsection shows a first attempt for the design of the dual polarized feed and even though the results obtained are good, it is possible to improve some aspects of the design by introducing some changes. This new design is based on the broadband offset quad-ridged waveguide orthomode transducer shown in [25]. The main modification with respect to the previous design consist in the excitation of each polarization in sections with different configurations of the ridges, see Fig. 3.1.12 in

order to avoid the excitation of the higher order mode TE_{11}

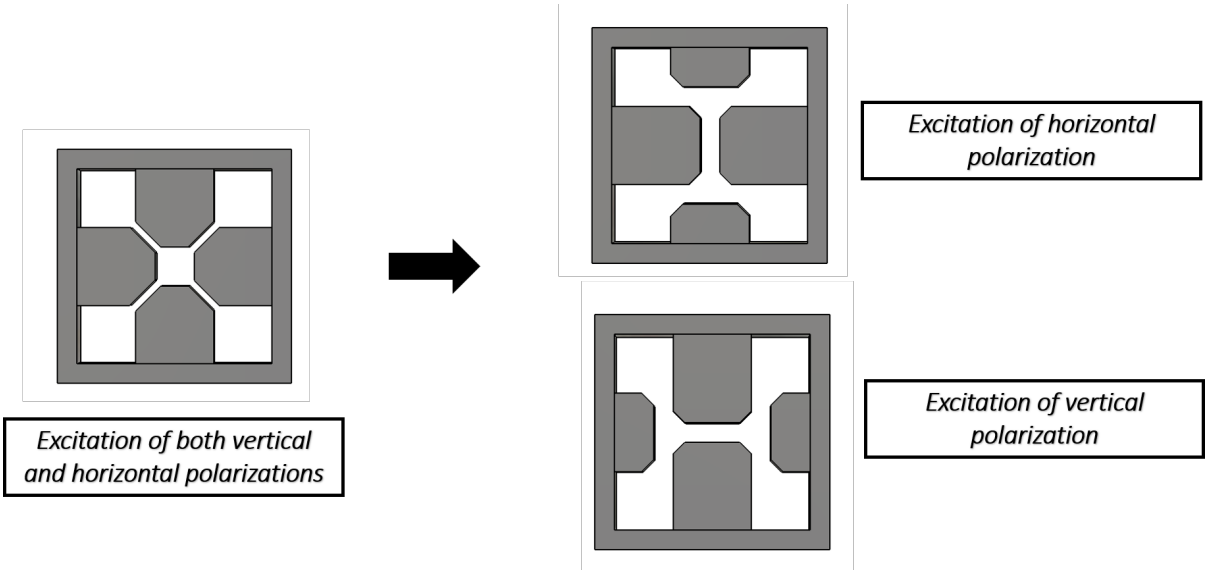

Figure 3.1.12: Changes with respect to the first design. Two different sections are used in order to excite the different polarizations.

The main objective with these changes is to increase as much as possible the cut-off frequency of the higher order mode TE_{11} so that it is not excited inside the waveguide. The cut off frequency of the first modes can be seen in Fig. 3.1.13. It can be noticed how the cut-off frequency of the fundamental mode is even lower than for the previous configuration, since the distance between the ridges is smaller, and also the cut-off frequency of the next mode is well above the one of the fundamental mode.

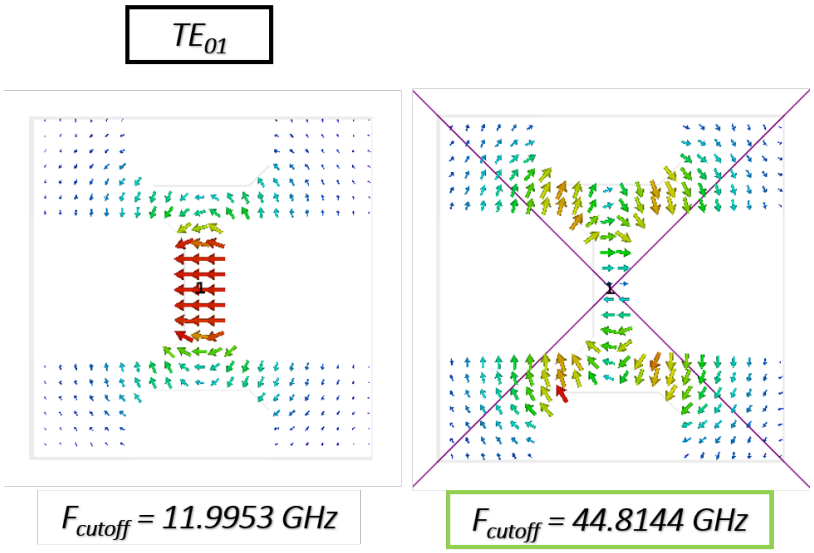

Figure 3.1.13: Cut-off frequencies for the first modes inside the new configuration of QRWG

The structure used for the final design of the dual-polarized feed can be seen in Fig. 3.1.14. It can be shown how after the cavity, there is a first section (1) where the horizontal ridges are closer than the vertical ones in order to excite the horizontal polarization. Then, in (2) the distance between the horizontal ridges starts to increase while the opposite happens to the vertical ridges so that the vertical polarization can be excited in (3). In the last part of the structure (4), the distance between the vertical ridges starts to increase again until it is the same than the distance between the horizontal ridges at the aperture of the feed.

Since the distance from the vertical port to the backshort is too long compared to the first design, the solution based on including a pin in the backshort cavity is not working in this structure. However, an alternative solution based on the introduction of a metal plate between the vertical ridges at the beginning of section (3) is used in this case in order to achieve a good impedance matching for both ports.

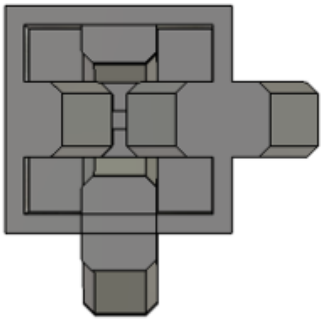

(a)

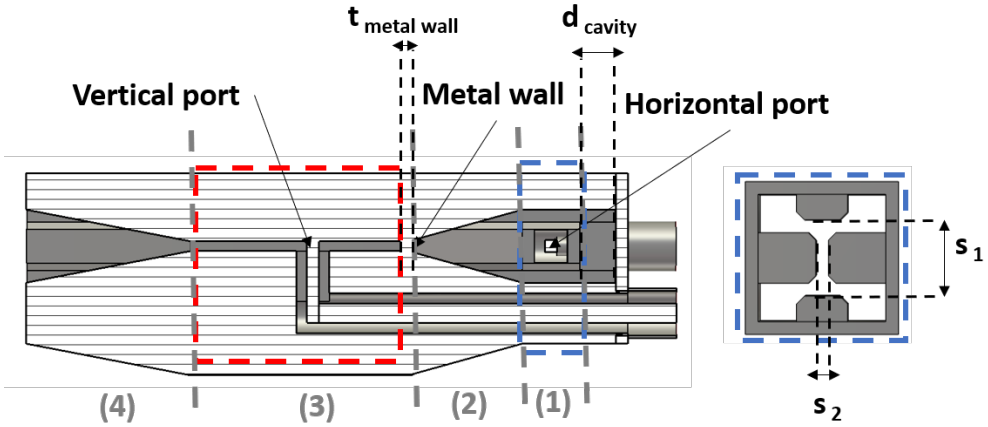

(b)

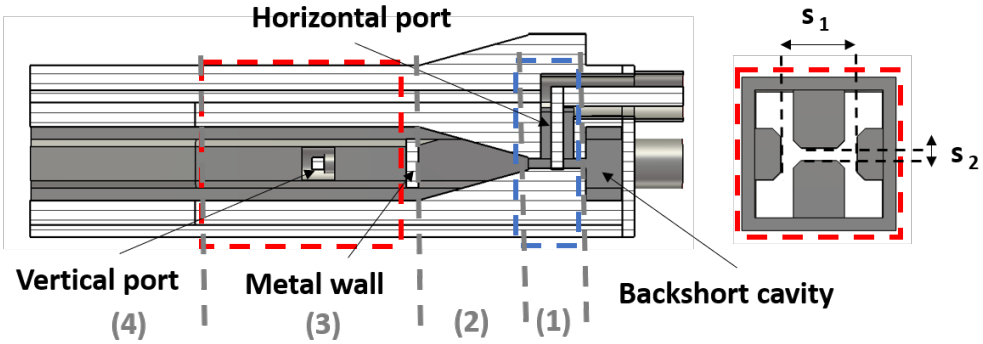

(c)

Figure 3.1.14: Final design of the dual-polarized feed. a) Front view, b) cross-section side view and c) cross-section top view

The results for the S-parameters of the new structure when radiating to free space can be seen in Fig. 3.1.15. it can be noticed in the results how not only both ports have a good matching from around 26 to 30 GHz, but also the isolation between them is good when radiating to free space. These results show some improvements with respect to the first design shown in the previous section.

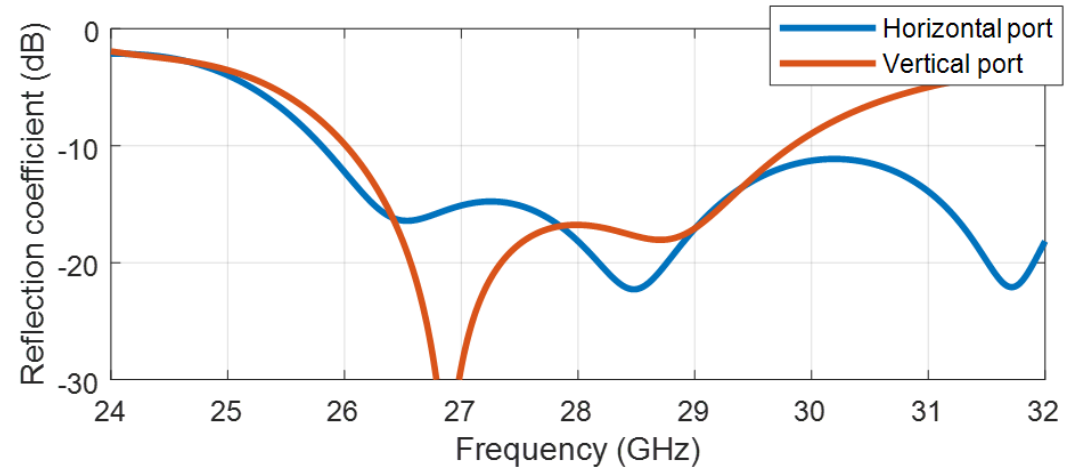

(a)

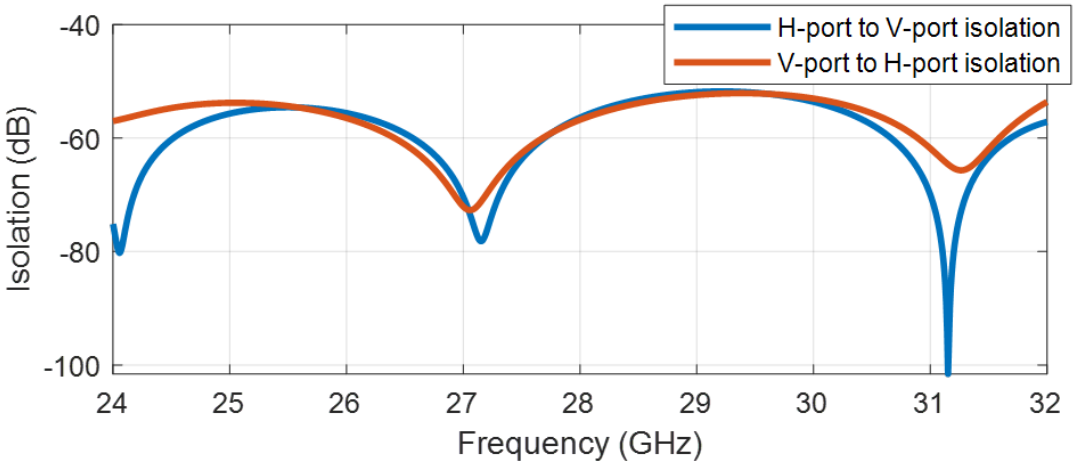

(b)

Figure 3.1.15: Results of the S-parameters for the final design of the dual-polarized feed when radiating to free space. The dimensions are $d_{backshort\,H-port} = 2.4mm$, $d_{metal\,wall\,V-port} = 3.6mm$, $w_{pin} = 0.5mm$, $s_1 = 3mm$, $s_2 = 0.5mm$, $w_1 = 2mm$, $w_2 = 1.4mm$, $d_{inner} = 0.8mm$, $D_{outer} = 1.85mm$, $r_{air\,gap} = 0.825mm$, $t_{metal\,wall} = 0.5mm$, $w_{gap\,pin} = 0.425mm$, $a = 5mm$, $s_{cavity} = 3mm$, $d_{cavity} = 1.9mm$, $l_{(1)} = 2.35mm$, $l_{(2)} = 4.6mm$, $l_{(3)} = 9.125mm$, $l_{(4)} = 6.5mm$, $s_{taper} = 3mm$

The 3D radiation pattern of the dual-polarized feed can be seen in Fig. 3.1.16

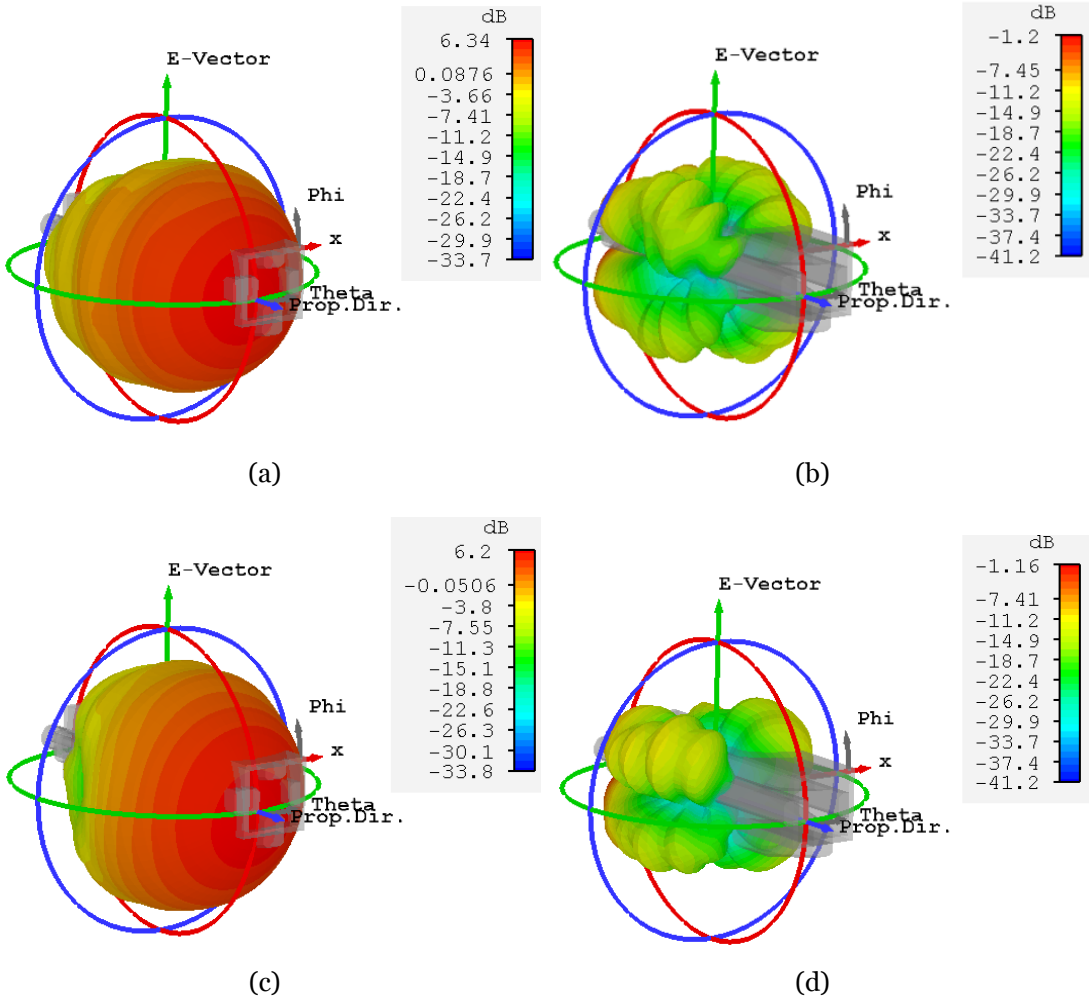

Figure 3.1.16: 3D radiation pattern of the final design of the dual-polarized feed at 28 GHz: a) Co-Pol horizontal port, b) cross-Pol horizontal port, c) co-Pol vertical port and d) cross-Pol vertical port

In Fig. 3.1.17, it can be seen a 2D representation of the radiation pattern for different frequencies. In this figure, the value of ϕ is keeps constant at 45°in order to show the main peaks of the cross-polarization.

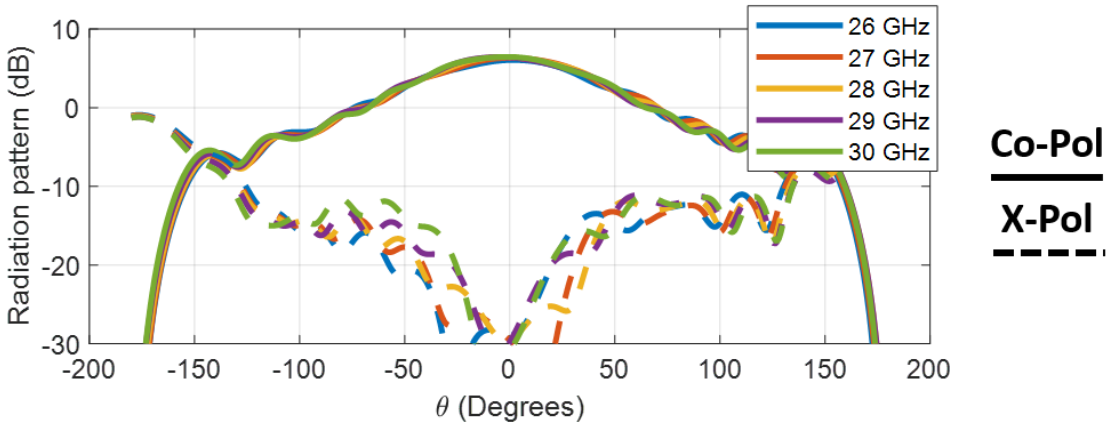

(a)

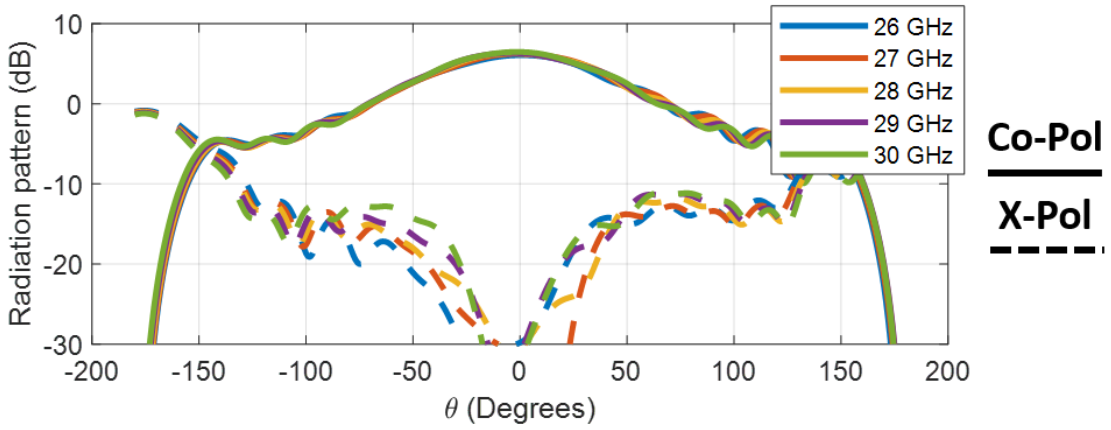

(b)

Figure 3.1.17: 2D representation of the radiation pattern for the final design of the dual-polarized feed at 28 GHz ($\phi = 45°$): a) Horizontal port and b) Vertical port

It can be seen in the results shown above how the cross-polarization level is more uniform for the different frequency values in comparison to the results of the first design. It is due to the fact that only the desired fundamental mode is being excited inside the QRWG and as a consequence of that, the electric field is more uniform at the aperture of the feed.

3.2 Gutman lens

As it has been said previously, a Gutman lens has been designed in this thesis. The main reasons to choose this lens is that first, its rotationally-symmetry enables beam steering capabilities; its size is smaller than other similar lenses such as the Luneberg lens; and it can be used with a dual-polarized feed.

The first step is to establish the parameters of the lens by using the Eq. 2.5. In this case, the value of the refractive index at the center of the lens is chosen to be $n(0) = \sqrt{3}$ in order to coincide with the refractive index of one of the dielectric material available from Premix [26]. The refractive index at the focal point was chosen to be $n(f) = \sqrt{2}$. A smaller value would reduce the reflections at the aperture of the dual-polarized feed but would increase the radius of the focal point, thus making the design less compact. On the other hand, a higher value would make the design more compact but would increase the reflections. With the values of the refractive index at the border and at the center of the lens it is possible to calculate the position of the focal point as a function of the radius of the lens. In this case the value of the radius for the focal point would be $f = \sqrt{2}R_{lens}/2$. Once done, it is necessary to establish a value for the radius of the lens, as it is known the value of the maximum directivity that it is possible to get with an antenna will depend on the aperture of it according to the next formula

$$D_{max} = \frac{4\pi}{\lambda^2} A \tag{3.1}$$

being A the value of the area of a circle with the same radius than the lens. Taking all of this into account, if the maximum value of the directivity is established to be $D_{max} = 27dB$, the radius of the Gutman lens must be $R_{lens} = 38mm$.

3.2.1 Unit cell

Once all the different parameters of the Gutman lens are known, it is possible to know the exact value of the refractive index at each position of the lens. However, it is not possible to build dielectric gradient index lenses in real life but they must undergo a discretization process first. That discretization process consists basically in the creation of different unit cells whose size must be small compared to the wavelength so that there is a certain periodicity. By changing the dielectric material density in each one of this unit cells, it is possible to obtain a different value of the effective refractive index . The size of the unit cell must be small enough compared to the wavelength in order to satisfy the homogeneity condition. However, since the purpose of this project is to design a lens which can be manufactured by using a 3D printer, the size must be

big enough so that it can be printable by using this technology. Taking all of this into account, the chosen size of the unit cell chosen is 3 mm. The unit cell, see Fig. 3.2.1, has a cubic shape from which a cubic cavity has been removed inside.

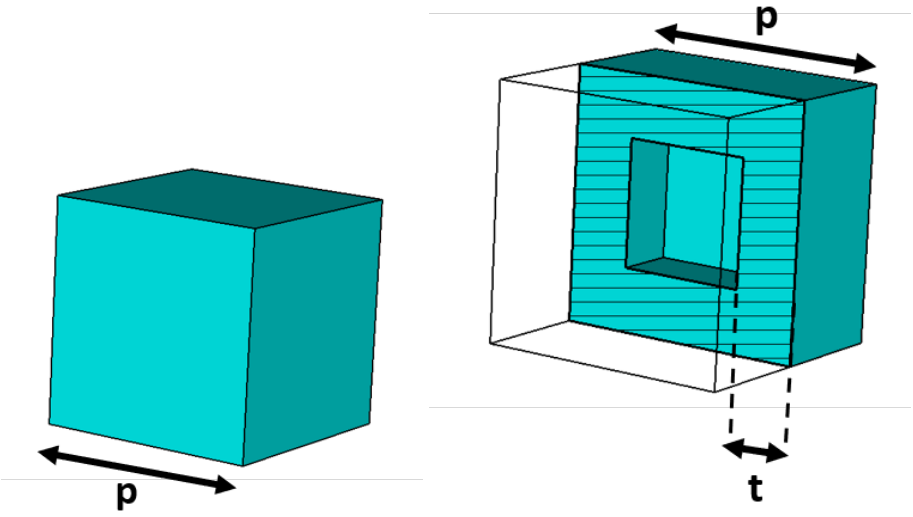

(a) (b)

Figure 3.2.1: Cubic unit cell: a) perspective view and b) side cross-sectional view

The next step after building and deciding the shape of the unit cell is to simulate its behaviour in order to model the value of n_{eff} as a function of t. This is done by using Eigenmode Mode of CST in order to obtain the dispersion diagram for all the different directions of the Irreducible Brillouin Zone (IBZ), see Fig 3.2.2. The IBZ is the minimum section of the unit cell which can be used in order to obtain the response of whole unit cell, . Since the dispersion diagram of a periodic structure is symmetric, it is only necessary to analyze the dispersion in the smallest repeatable section. [27]

Once done that, MATLAB is used in order to process all the previous data. The refractive index can be obtained by using the next formula

$$\beta = \frac{phase}{p} = \frac{2\pi}{\lambda} = \frac{2\pi}{(\frac{c}{fn_{eff}})} \tag{3.2}$$

Once applied the formula shown above, the value of the effective refractive index n_{eff}

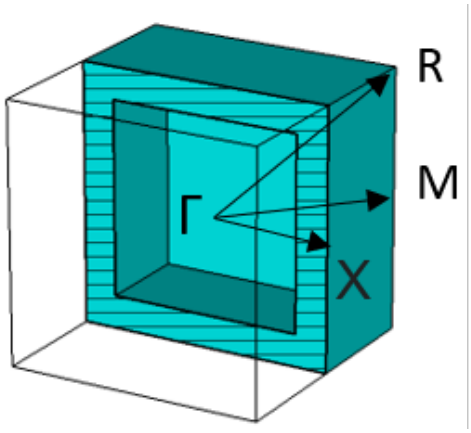

Figure 3.2.2: Critical points for the IBZ of the unit cell. Γ is the center of the cube, X is the center of a face, M is the center of an edge and R is a corner point.

is obtained as a function of the thickness of the unit cell t, see Fig. 3.2.3. The value of the effective refractive index is shown for the different directions of the IBZ in order to check how isotropic the unit cell is.

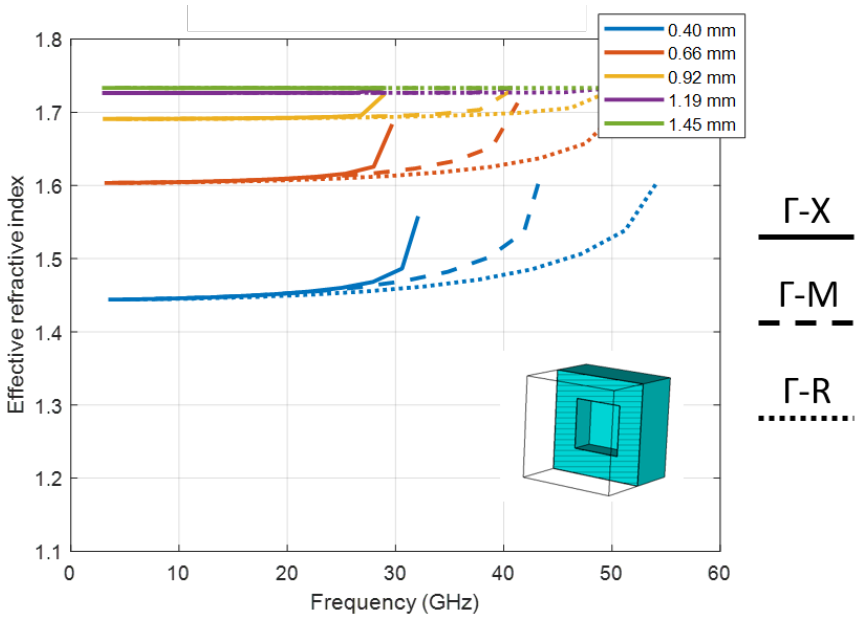

Figure 3.2.3: Effective refractive index of the unit cell as a function of the thickness

In the picture above it can be seen how the refractive index also depends on the frequency. This dispersion of the effective refractive index is due to the periodicity.

Once the effective refractive index of the unit cell as a function of thickness has been obtained, it is time to build the lens. For that purpose, MATLAB was used in order to control CST and place each unit cell with a certain thickness at each specific position

according to the required refractive index. The 3D model of the designed Gutman lens can be seen in Fig. 3.2.4. In can be seen in the picture how a small portion of the Gutman lens has been removed in order to place the dual-polarized feed at the focal point located inside the lens.

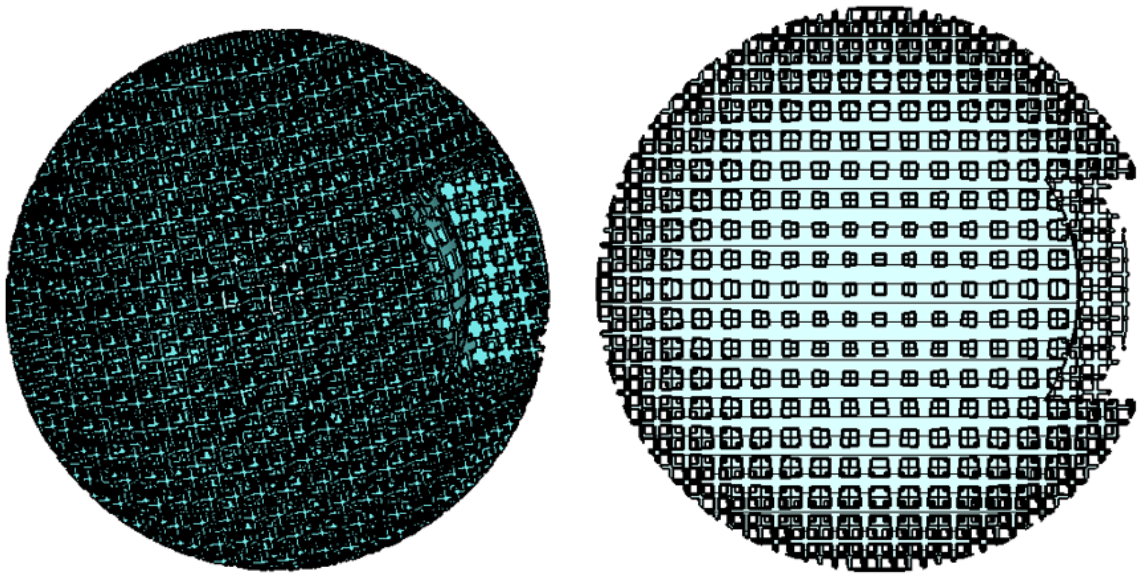

(a) (b)

Figure 3.2.4: 3D model of the designed Gutman lens: a) Perspective view, b) cross-section side view.

Chapter 4

Results

The main goal of this chapter is to show the simulation results of the final design of the dual-polarized lens antenna including both the dual-polarized feed based on a QRWG and the Gutman lens.

Some changes had to be performed on the dual-polarized feed. The design shown in the previous chapter was radiating to free space. However, that is not the case anymore since the permittivity at the focal point of the designed Gutman lens is 2. As a consequence of that, it was necessary to modify the aperture of the feed. By reducing the distance between the ridges at the aperture, s_{taper} from 3 mm to 2.8 mm, the wave impedance at the aperture of the feed decreases, and so does the reflections as can be seen in Fig. 4.0.1.

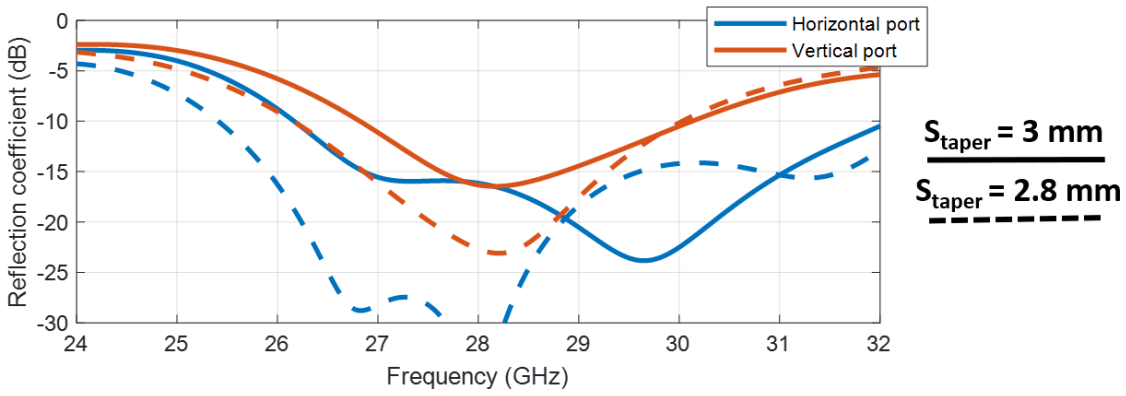

Figure 4.0.1: Improvement of the reflection coefficient after reducing the distance between the ridges at the aperture, s_{taper}, from 3 mm to 2.8 mm.

The array is composed by 9 different dual-polarized feeds, see Fig. 4.0.2. By feeding each specific port of the array, it is possible to change the direction of the main lobe of the radiation pattern. It can be seen how there is a curvature at the aperture of the array with the same radius than the focal point of the Gutman lens.

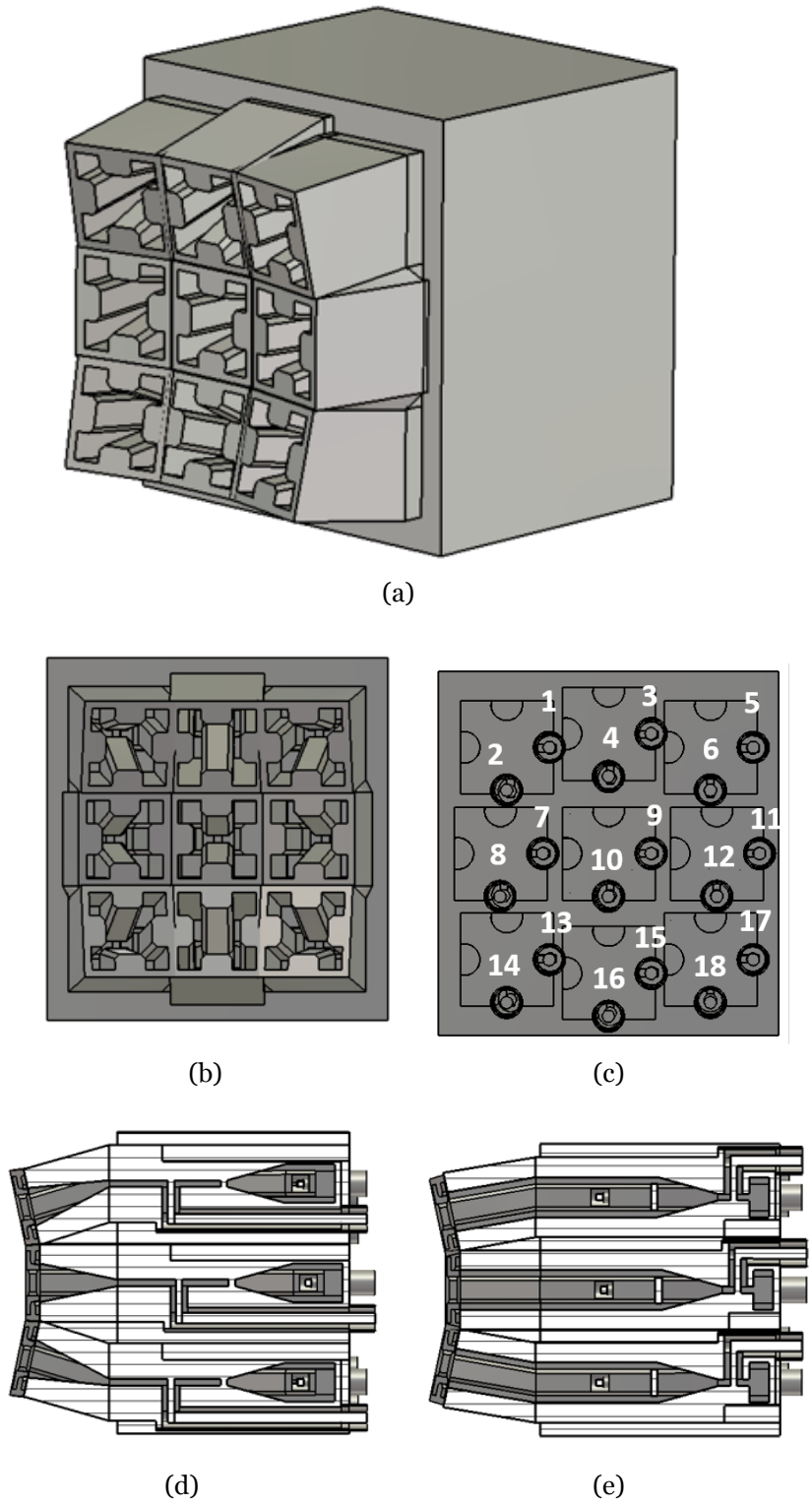

Figure 4.0.2: Dual-polarized array feed: a) Perspective view, b) front view, c) back view with port numbers, d) cross-section side view and e) cross-section top view

The next figure shows the lens antenna composed by the dual-polarized feed and the Gutman lens. It can be seen how the dual-polarized array feed is placed at the focal point located inside the lens.

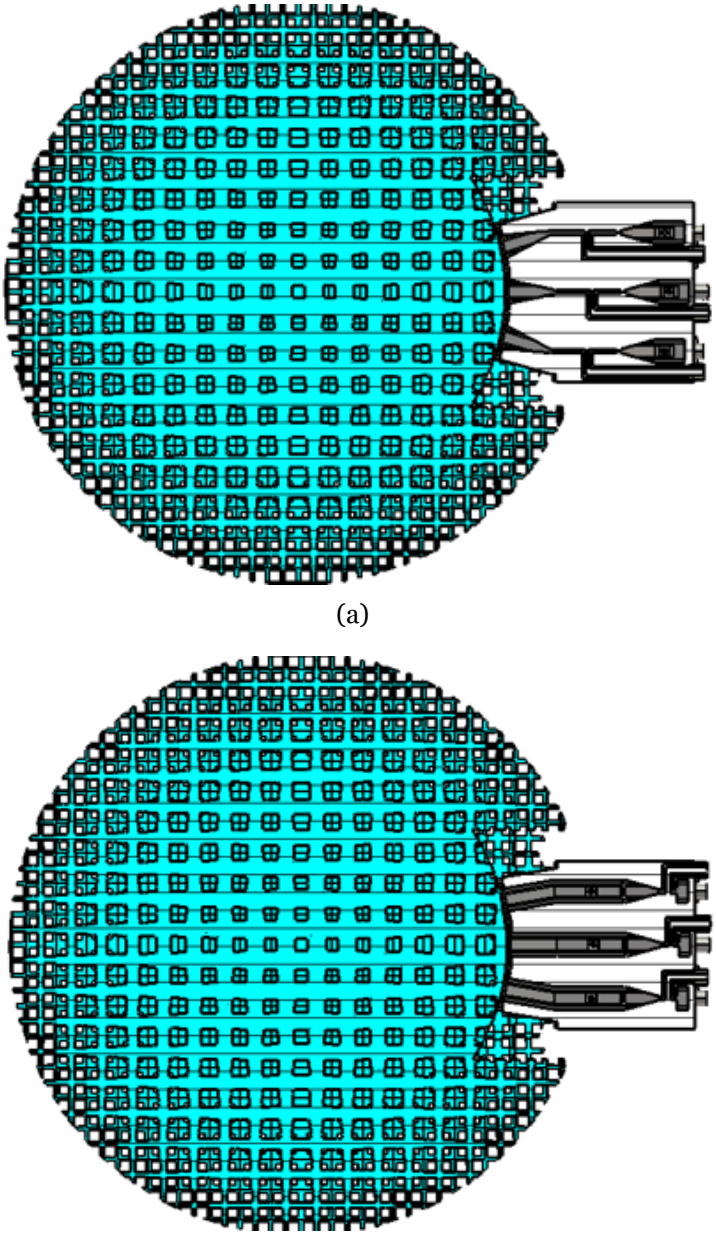

(a)

(b)

Figure 4.0.3: Dual-polarized array feed and Gutman lens: a) Cross-section side view a b) cross-section top view

Once built the structure, the next step was to simulate the results for the S-parameters of the lens antenna in order to see if it met the initial requirements. However, the complexity of the design made it difficult to simulate the whole system due to the high computational cost. In order to run the simulation, a simple model of the Gutman lens

based on cubes of a specific permittivity was created in order to reduce the simulation time. The results for the S-parameters of 4 different ports of the dual-polarized array can be seen in 4.0.4. It can be seen how there is a good matching from around 26.7 to 30 GHz. The worst results correspond to the port 9 and 10, which are located in the middle of the array. It can also be noticed how the isolation between the ports is lower than -50 dB.

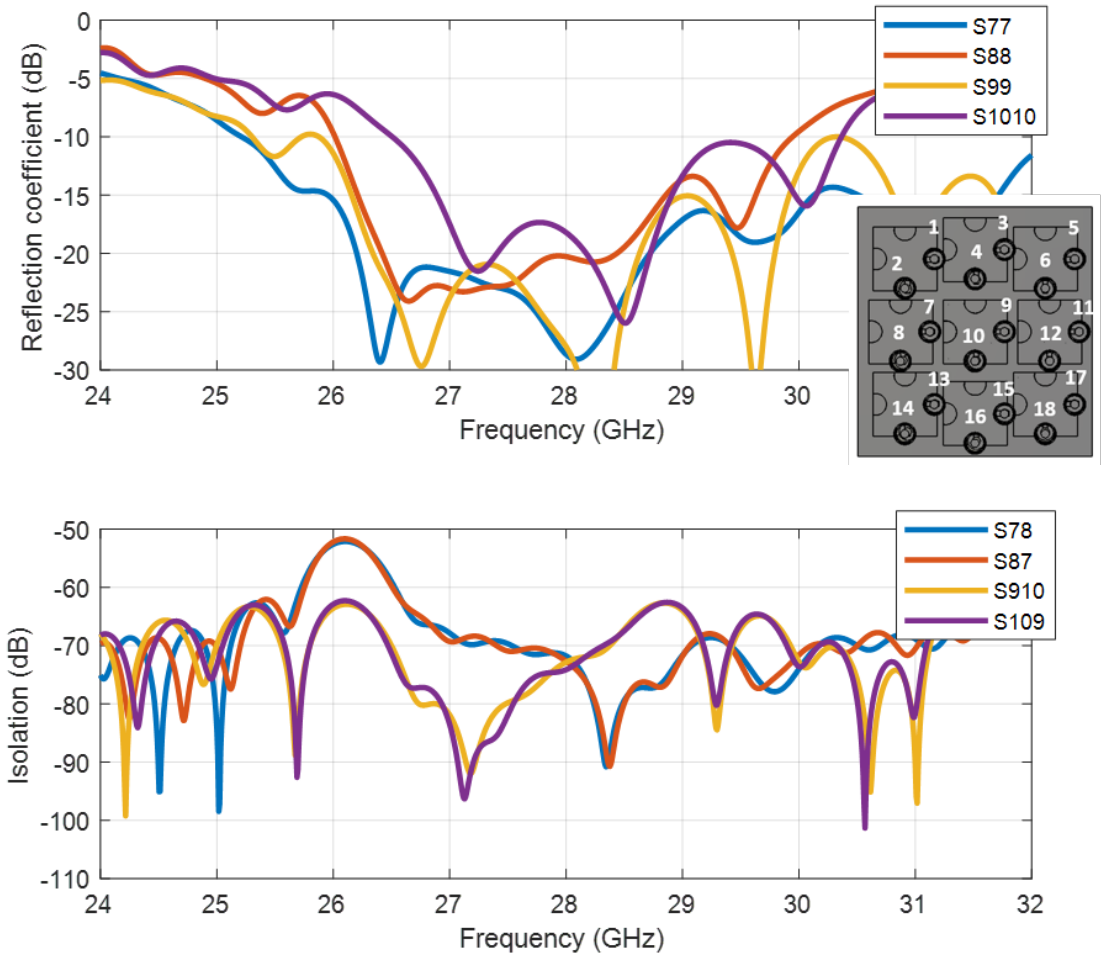

Figure 4.0.4: Dual-polarized array feed: a) Perspective view, b) front view, c) back view, d) cross-section side view and e) cross-section top view

In Fig. 4.0.5 it can be seen how the Gutman lens turns the spherical wave coming from the dual-polarized array feed into a planar wave.

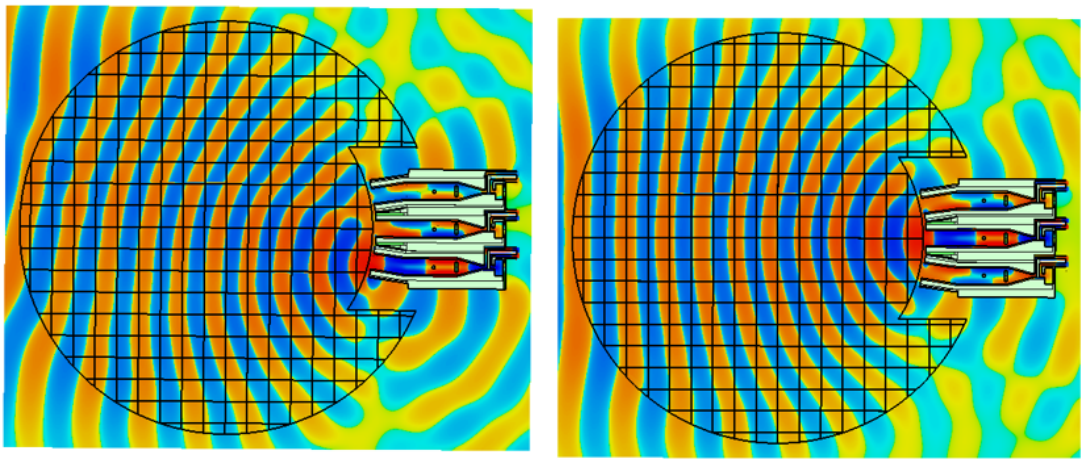

(a) (b)

Figure 4.0.5: Cross-sectional top view of the electric field in the Gutman lens: a) Port 8 and b) Port 10

The last step in order to check that the design was working properly, was to check the far field results of the dual-polarized lens antenna. The 3D radiation pattern can be seen in Fig. 4.0.6. It can be noticed how, by placing the Gutman lens in front of the aperture of the feed, it is possible to generate a very directive beam focused in one specific direction. It must be noted how the Gutman lens also increases the level of the four beams in the cross-polarization. However, the level of the cross-polarization is still low compared to the co-polarization.

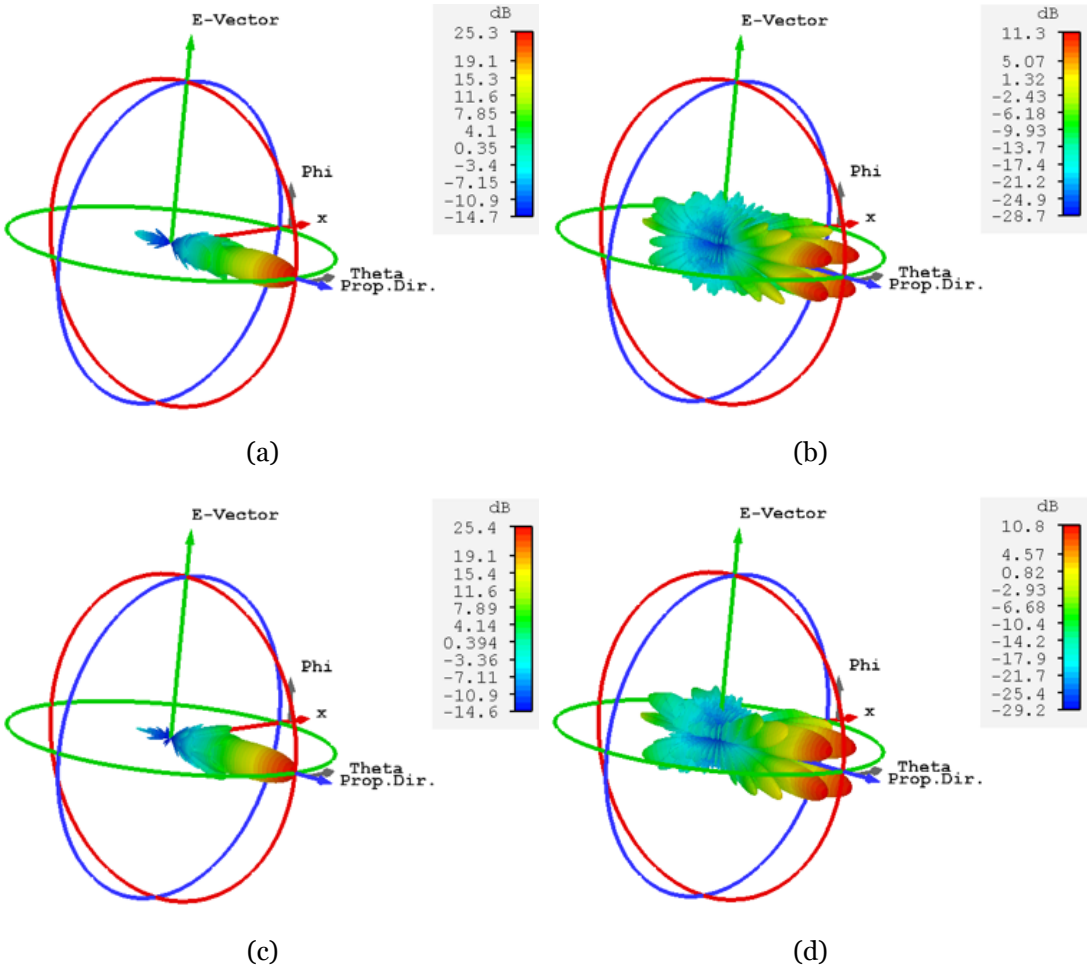

Figure 4.0.6: 3D radiation pattern of the dual-polarized lens antenna at 28 GHz: a) Port 9 Co-Pol , b) Port 9 X-Pol, c) Port 10 Co-Pol and d) Port 10 X-Pol

In Fig. 4.0.8, it can be seen a 2D representation of the radiation pattern. In this figure, the value of ϕ is kept constant at 45°in order to show the main peaks of the cross-polarization.

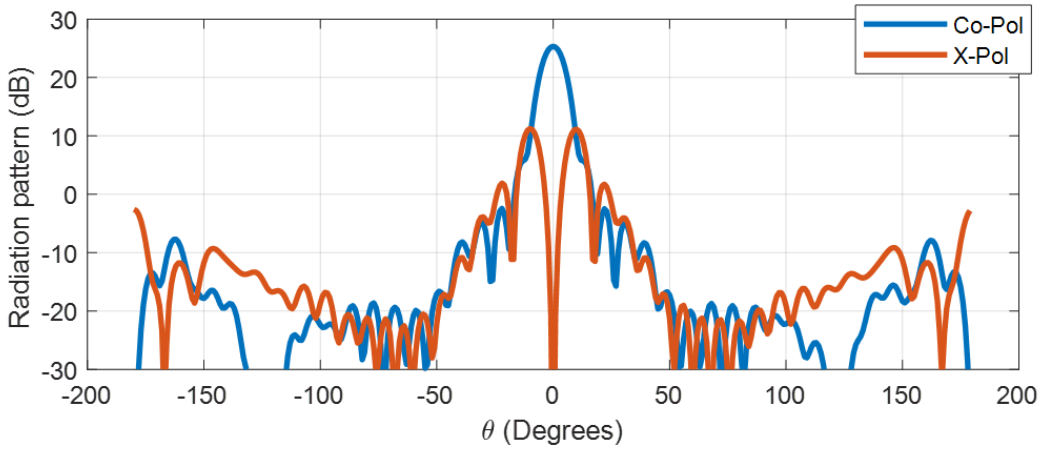

(a)

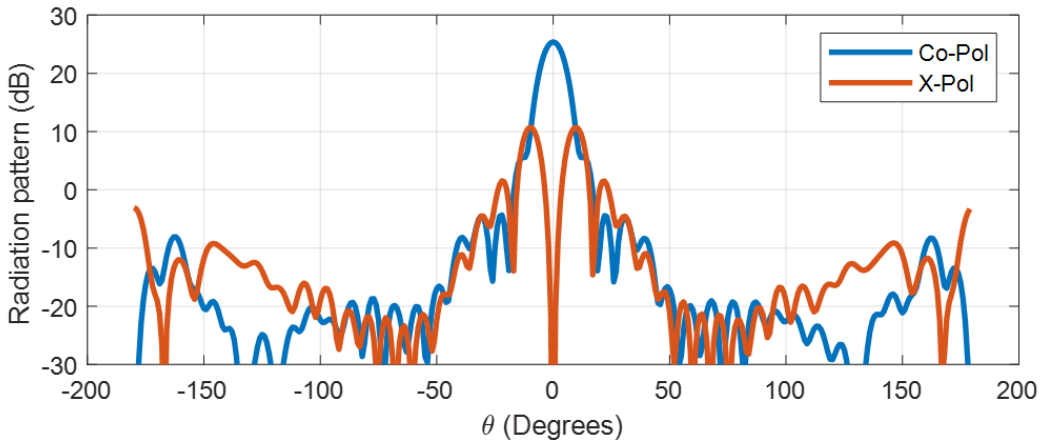

(b)

Figure 4.0.7: 2D representation of the radiation pattern for the dual-polarized lens antenna at 28 GHz ($\phi = 45°$): a) Port 9 and b) Port 10

As it was explained previously, one important requirement for the antennas used in the future 5G communication networks is the ability to reconfigure their radiation pattern. By changing the feeding port of the dual-polarized array feed, it is possible to steer the beam. In Fig. 4.0.8, it can be seen a 2D representation of the radiation pattern. In this figure, the value of ϕ is kept constant at 0°in order to show the beam steering in azimuth.

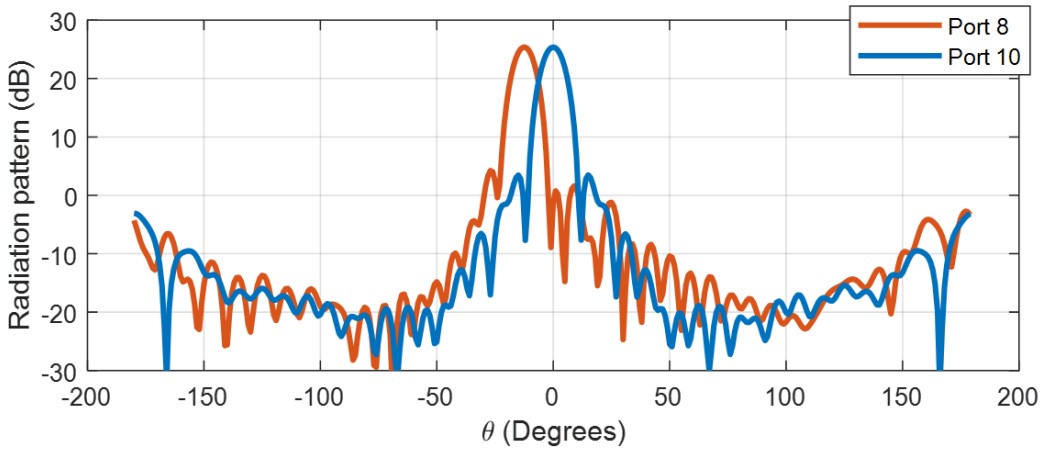

(a)

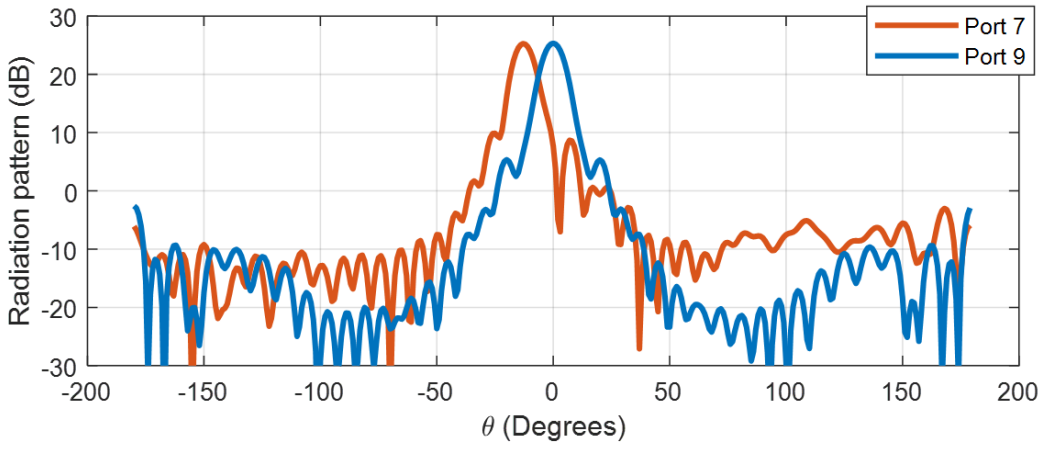

(b)

Figure 4.0.8: 2D representation of the radiation pattern for the dual-polarized lens antenna at 28 GHz ($\phi = 45°$): a) Port 9 and b) Port 10

Chapter 5

Manufacturing

The next step after checking that the simulation results of the dual-polarized feed were good enough was to manufacture a real prototype in order to be able to measure and see the actual performance of the feed. Due to the complexity of the structure, the method chosen in order to manufacture the prototype was metal 3D printing.

5.1 Prototype

After sending the original prototype to several companies and once received the feedback of all of them, it was confirmed that the prototype could not be manufactured as it was. There are several features in the structure which made this design not suitable to be manufactured by using 3D printing technology. It can be seen how the thin pins used to excite both polarizations are hanging at 90º without any support below, see Fig. 5.1.1. Due to the latter, these features could bend or break during the manufacturing process.

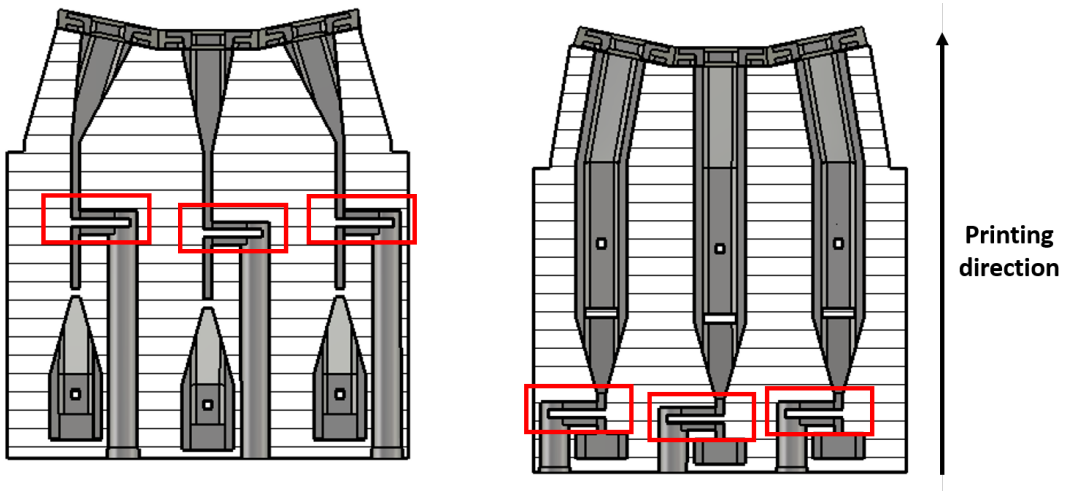

(a) (b)

Figure 5.1.1: Cross-section side view showing the pins hanging at 90º which make the structure not suitable to be 3D printed

Some changes were performed to the prototype in order to make feasible its manufacture. The first one consisted in dividing the structure in three different parts, see Fig. 5.1.2. A support layer is introduced in between each part in such a way that the pins have a support below. The idea is to print these support layers in a material which can be easily removed after the manufacturing process. The final structure would be assembled by using screws in order to tight the three different pieces together.

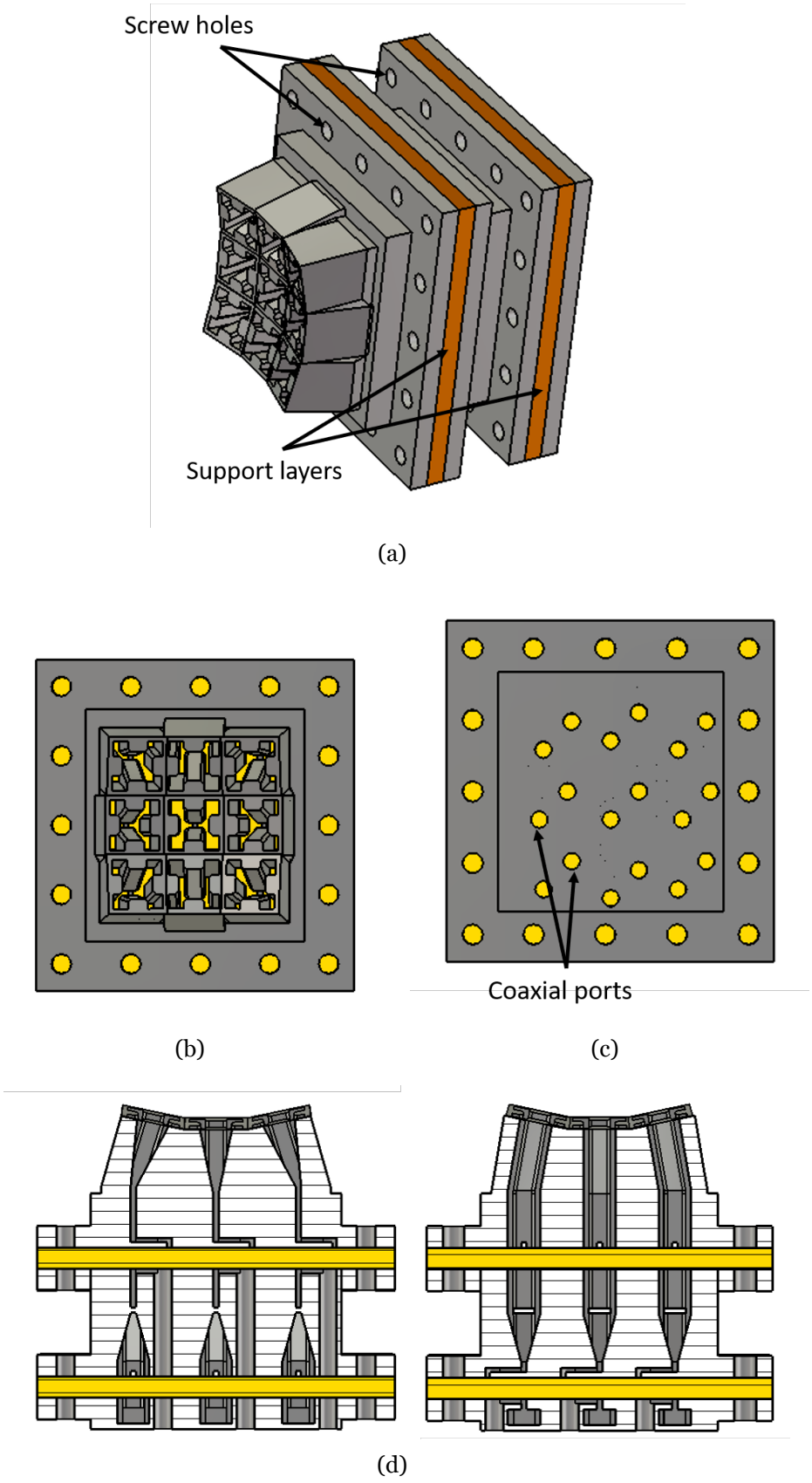

Figure 5.1.2: Prototype idea to be manufactured: a) Perspective view, b) top view, c) bottom view and d) cross-section side views

5.2 Tolerance analysis

It was also necessary to perform a tolerance analysis in order to have an idea of how much the manufacturing tolerances would affect the results. Only the most critical dimensions were analyzed. It can be noticed how the manufacturing tolerances should be smaller than ±0.1 mm in order to keep the results for the dual-polarized feed almost constant.

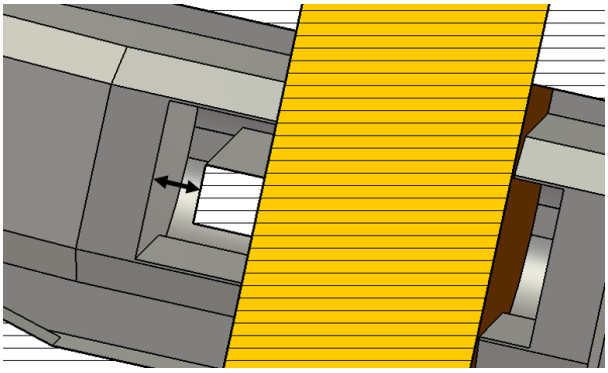

(a)

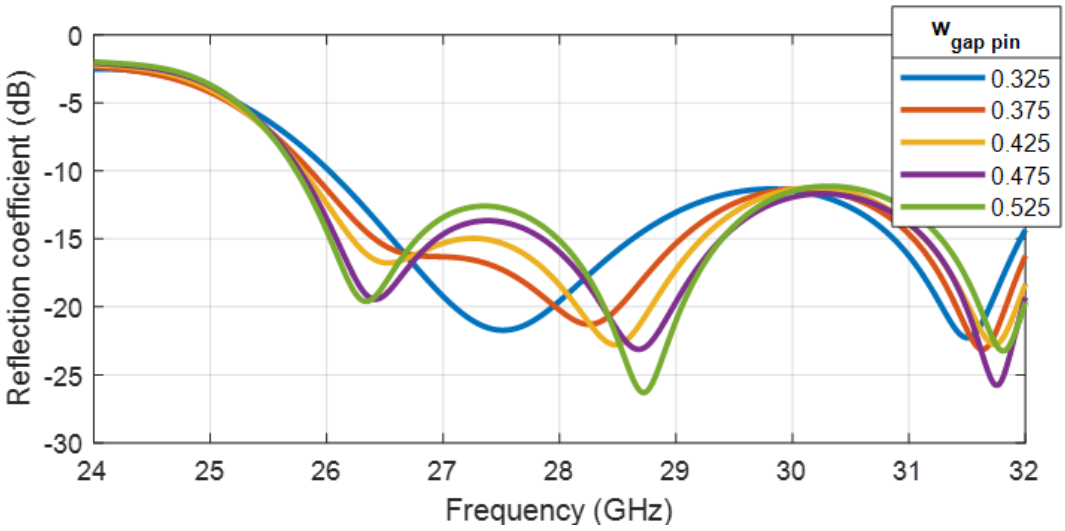

(b)

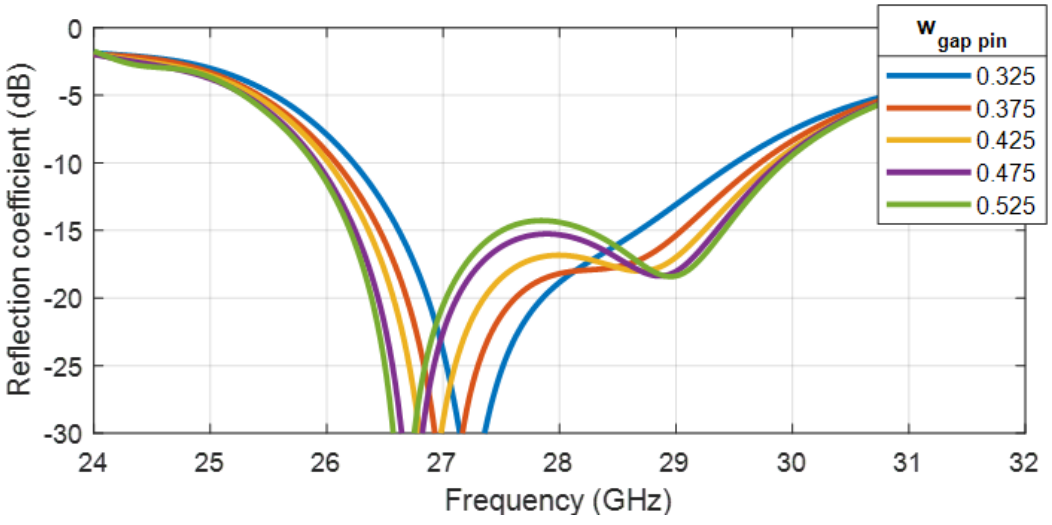

(c)

Figure 5.2.1: Tolerance analysis for the distance between the pin and the cavity $w_{gap\,pin}$: a) Prototype view, b) horizontal port and c) vertical port

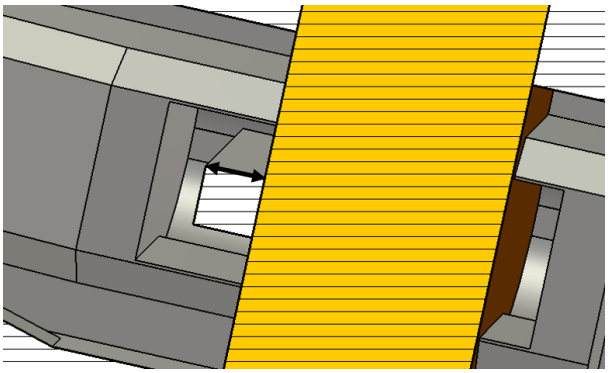

(a)

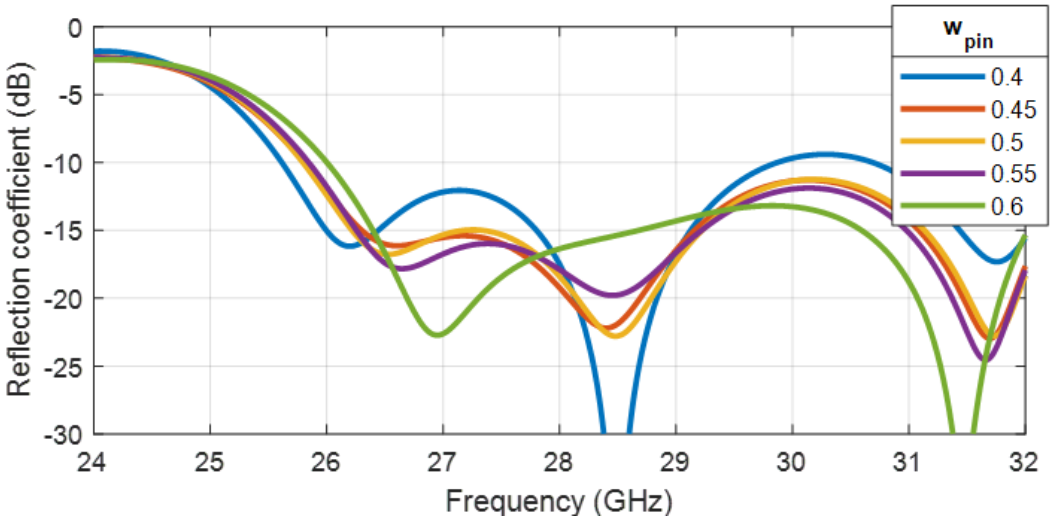

(b)

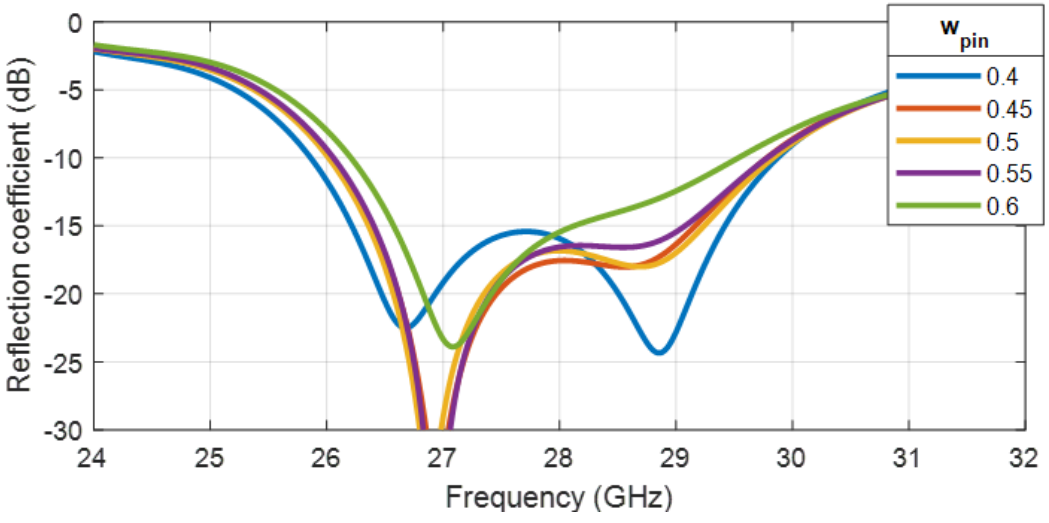

(c)

Figure 5.2.2: Tolerance analysis for the width of the pin w_{pin}: a) Prototype view, b) horizontal port and c) vertical port

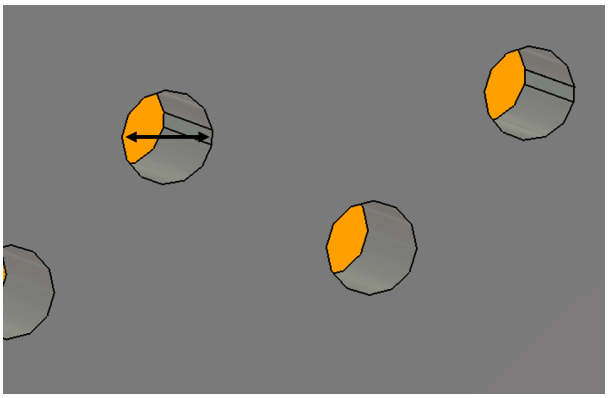

(a)

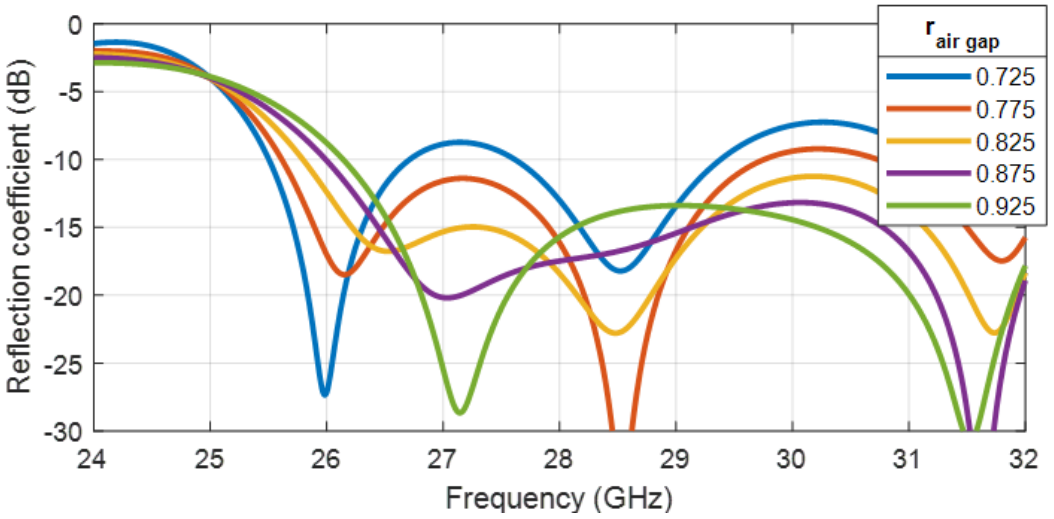

(b)

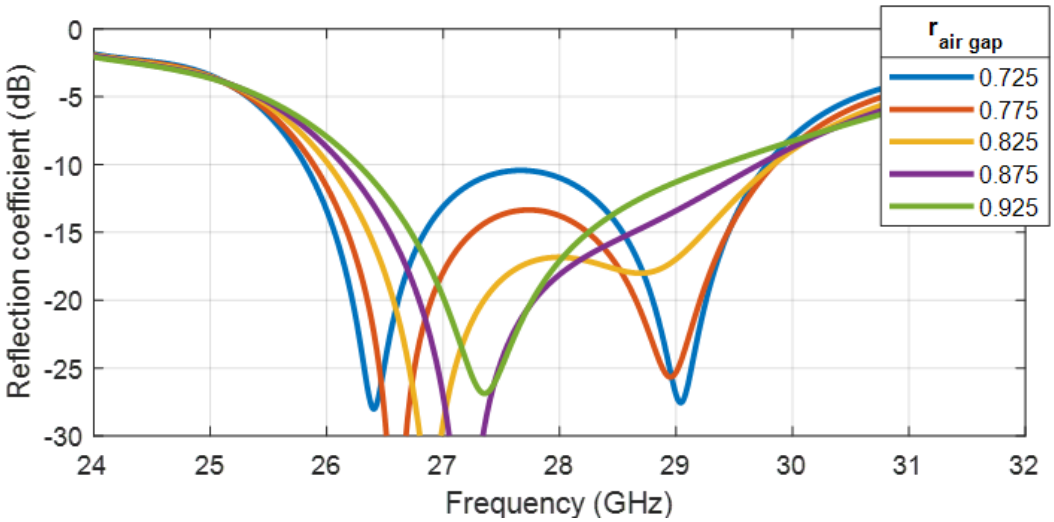

(c)

Figure 5.2.3: Tolerance analysis for the radius of the cylindrical cavity $r_{air\,gap}$: a) Prototype view, b) horizontal port and c) vertical port

Chapter 6

Conclusions and Future Work

In this thesis, a compact dual-polarized array feed to be used in mmWave lens antennas for the future 5G communication systems has been designed. A Gutman lens was also designed in order to be placed at the aperture of the feed. The simulation results for the final version of the dual-polarized array feed are promising. The reflection coefficient is lower than -10 dB from around 26.7 to 30 GHz, thus meeting the bandwidth requirement. The gain of the lens antenna is around 25.3 dBi at 28 GHz. The isolation between the ports is smaller than -50 dB in the frequency band of operation.

A prototype of the dual-polarized array feed was sent to many companies in order to be manufactured. The small features, some of them around 0.5 mm, along with the low tolerance of the design, made this design very difficult to be manufactured. However, some changes were performed to the original design. The structure was divided in three different pieces separated so that each one of them can be manufactured separately. After the manufacturing, the three separated pieces can be assembled together by using screws.

There are several future line of works on this project. The main one is to manufacture the prototype in order to measure it and check the actual performance of the feed. Another line of work would be the further optimization of the structure in every step in order to maximize the operation bandwidth. Regarding the manufacturing, some features in the design might be changed in order to make this design suitable to be printed in one piece, thus making the manufacturing process easier.

Bibliography

[1] *What is 5G? Do you want to know more about 5G?* Mar. 2020. URL: https://www.ericsson.com/en/5g/what-is-5g.

[2] *Bringing 5G networks indoors: Whitepaper*. Apr. 2020. URL: https://www.ericsson.com/en/reports-and-papers/white-papers/bringing-5g-networks-indoors.

[3] Quevedo-Teruel, O., Ebrahimpouri, M., and Ghasemifard, F. "Lens Antennas for 5G Communications Systems". In: *IEEE Communications Magazine* 56.7 (2018), pp. 36–41.

[4] *Bringing 5G networks indoors: Whitepaper*. 2015. URL: https://www.etsi.org/images/files/ETSITechnologyLeaflets/MillimetreWaveTransmission.pdf.

[5] Wang, Y., Li, J., Huang, L., Jing, Y., Georgakopoulos, A., and Demestichas, P. "5G Mobile: Spectrum Broadening to Higher-Frequency Bands to Support High Data Rates". In: *IEEE Vehicular Technology Magazine* 9.3 (2014), pp. 39–46.

[6] Collin, Robert E. "Chapter 3: Transmission Lines and Waveguides". In: *Field theory of guided waves*. McGraw-Hill, 1960.

[7] Pozar, D.M. *Microwave Engineering*. Wiley, 2004. ISBN: 9780471448785. URL: https://books.google.se/books?id=4wzpQwAACAAJ.

[8] Cohn, S. B. "Properties of Ridge Wave Guide". In: *Proceedings of the IRE* 35.8 (1947), pp. 783–788.

[9] Hopfer, S. "The Design of Ridged Waveguides". In: *IRE Transactions on Microwave Theory and Techniques* 3.5 (1955), pp. 20–29.

[10] Weimin Sun and Balanis, C. A. “MFIE analysis and design of ridged waveguides”. In: *IEEE Transactions on Microwave Theory and Techniques* 41.11 (1993), pp. 1965–1971.

[11] Sun, W. and Balanis, C. A. “Analysis and design of quadruple-ridged waveguides”. In: *IEEE Transactions on Microwave Theory and Techniques* 42.12 (1994), pp. 2201–2207.

[12] Liu, Jun, Lin, Gao, Li, Jianbo, and Zhong, Hong. “Analysis of quadruple corner-cut ridged square waveguide using a scaled boundary finite element method”. In: *Applied Mathematical Modelling* 36.10 (2012), pp. 4797–4809. ISSN: 0307-904X. DOI: https://doi.org/10.1016/j.apm.2011.12.015. URL: http://www.sciencedirect.com/science/article/pii/S0307904X11008018.

[13] Zhongxiang Shen and Chao Feng. “A new dual-polarized broadband horn antenna”. In: *IEEE Antennas and Wireless Propagation Letters* 4 (2005), pp. 270–273.

[14] Pedrotti, L.S. *Fundamentals of Photonics: Basic geometrical optics. Module 1,3*. SPIE, 2010. URL: https://books.google.se/books?id=3NgSyAEACAAJ.

[15] Farkas, Henrik, Kály-Kullai, Kristóf, and Sieniutycz, Stanislaw. “Chapter 17 - The Fermat Principle and Chemical Waves”. In: *Variational and Extremum Principles in Macroscopic Systems*. Ed. by Stanislaw Sieniutycz and Henrik Farkas. Oxford: Elsevier, 2005, pp. 355–373. ISBN: 978-0-08-044488-8. DOI: https://doi.org/10.1016/B978-008044488-8/50020-5. URL: http://www.sciencedirect.com/science/article/pii/B9780080444888500205.

[16] Meyer-Arendt, Jurgen R. “Mathematical Theory of Optics. R. K. Luneburg. With a foreword by Emile Wolf and supplementary notes by M. Herzberger. University of California Press, Berkeley, 1964. xxx + 448 pp. Illus. 12.50”. In: *Science* 147.3663 (1965), pp. 1276–1277. ISSN: 0036-8075. DOI: 10.1126/science.147.3663.1276-a. eprint: https://science.sciencemag.org/content/147/3663/1276.2.full.pdf. URL: https://science.sciencemag.org/content/147/3663/1276.2.

[17] Maxwell, James Clerk. *”Solutions of problems” Cambridge Dublin Math. J. 8, 188–195*. 1854.

[18] Fuchs, B., Lafond, O., Rondineau, S., and Himdi, M. “Design and characterization of half Maxwell fish-eye lens antennas in millimeter waves”. In: *IEEE Transactions on Microwave Theory and Techniques* 54.6 (2006), pp. 2292–2300.

[19] Gutman, A. S. “Modified Luneberg Lens”. In: *Journal of Applied Physics* 25.7 (1954), pp. 855–859. DOI: 10.1063/1.1721757. eprint: https://doi.org/10.1063/1.1721757. URL: https://doi.org/10.1063/1.1721757.

[20] Quevedo-Teruel, Oscar, Tang, Wenxuan, Mitchell-Thomas, Rhiannon C., Dyke, Amy, Dyke, Hazel, Zhang, Lianhong, Haq, Sajad, and Hao, Yang. “Transformation optics for antennas: why limit the bandwidth with metamaterials?” In: *Scientific Reports* 3.1 (2013). DOI: 10.1038/srep01903.

[21] Leonhardt, Ulf. “Optical Conformal Mapping”. In: *Science* 312.5781 (2006), pp. 1777–1780. ISSN: 0036-8075. DOI: 10.1126/science.1126493. eprint: https://science.sciencemag.org/content/312/5781/1777.full.pdf. URL: https://science.sciencemag.org/content/312/5781/1777.

[22] Engheta, Nader and Ziolkowski, Richard W. *Metamaterials: Physics and Engineering Explorations*. English (US). John Wiley and Sons, Sept. 2006. ISBN: 0471761028. DOI: 10.1002/0471784192.

[23] Quevedo-Teruel, O., Ebrahimpouri, M., and Ng Mou Kehn, M. “Ultrawideband Metasurface Lenses Based on Off-Shifted Opposite Layers”. In: *IEEE Antennas and Wireless Propagation Letters* 15 (2016), pp. 484–487.

[24] Bjorkqvist, O., Zetterstrom, O., and Quevedo-Teruel, O. “Additive manufactured dielectric Gutman lens”. In: *Electronics Letters* 55.25 (2019), pp. 1318–1320.

[25] Villiers, D. I. L. D., Meyer, P., and Palmer, K. D. “Broadband offset quad-ridged waveguide orthomode transducer”. In: *Electronics Letters* 45.1 (2009), pp. 60–62.

[26] *Dielectric Materials with Ultra-low Losses Even at mmWaves: PREPERM®*. URL: https://www.preperm.com/.

[27] Joannopoulos, John D., Johnson, Steven G., Winn, Joshua N., and Meade, Robert D. *Photonic Crystals: Molding the Flow of Light (Second Edition)*. 2nd ed. Princeton University Press, 2008. ISBN: 0691124566. URL: http://www.amazon.com/Photonic-Crystals-Molding-Light-Second/dp/

0691124566%3FSubscriptionId%3D13CT5CVB80YFWJEPWS02%26tag%3Dws%26linkCode%3Dxm2%26camp%3D2025%26creative%3D165953%26creativeASIN%3D0691124566.